JACS
JOURNAL OF THE AMERICAN CHEMICAL SOCIETY
Article
pubs.acs.org/JACS

Influences of Dilute Organic Adsorbates on the Hydration of Low-Surface-Area Silicates

Rahul P. Sangodkar,[†] Benjamin J. Smith,[†] David Gajan,[‡] Aaron J. Rossini,[‡] Lawrence R. Roberts,[§] Gary P. Funkhouser,[∥] Anne Lesage,[‡] Lyndon Emsley,[‡,⊥] and Bradley F. Chmelka*[,†]

[†]Department of Chemical Engineering, University of California, Santa Barbara, California 93106, United States
[‡]Centre de RMN à Très Hauts Champs, Institut de Sciences Analytiques (CNRS/ENS Lyon/UCB Lyon 1), Université de Lyon, 69100 Villeurbanne, France
[§]Roberts Consulting Group, 44 Windsor Avenue, Acton, Massachusetts 01720, United States
[∥]Halliburton, 3000 North Sam Houston Parkway East, Houston, Texas 77032, United States
[⊥]Institut des Sciences et Ingénierie Chimiques, Ecole Polytechnique Fédérale de Lausanne (EPFL), CH-1015 Lausanne, Switzerland

Supporting Information

ABSTRACT: Competitive adsorption of dilute quantities of certain organic molecules and water at silicate surfaces strongly influence the rates of silicate dissolution, hydration, and crystallization. Here, we determine the molecular-level structures, compositions, and site-specific interactions of adsorbed organic molecules at low absolute bulk concentrations on heterogeneous silicate particle surfaces at early stages of hydration. Specifically, dilute quantities (~0.1% by weight of solids) of the disaccharide sucrose or industrially important phosphonic acid species slow dramatically the hydration of low-surface-area (~1 m^2/g) silicate particles. Here, the physicochemically distinct adsorption interactions of these organic species are established by using dynamic nuclear polarization (DNP) surface-enhanced solid-state NMR techniques. These measurements provide significantly improved signal sensitivity for near-surface species that is crucial for the detection and analysis of dilute adsorbed organic molecules and silicate species on low-surface-area particles, which until now have been infeasible to characterize. DNP-enhanced 2D $^{29}Si\{^1H\}$, $^{13}C\{^1H\}$, and $^{31}P\{^1H\}$ heteronuclear correlation and 1D $^{29}Si\{^{13}C\}$ rotational-echo double-resonance NMR measurements establish hydrogen-bond-mediated adsorption of sucrose at distinct nonhydrated and hydrated silicate surface sites and electrostatic interactions with surface Ca^{2+} cations. By comparison, phosphonic acid molecules are found to adsorb electrostatically at or near cationic calcium surface sites to form Ca^{2+}–phosphonate complexes. Although dilute quantities of both types of organic molecules effectively inhibit hydration, they do so by adsorbing in distinct ways that depend on their specific architectures and physicochemical interactions. The results demonstrate the feasibility of using DNP-enhanced NMR techniques to measure and assess dilute adsorbed molecules and their molecular interactions on low-surface-area materials, notably for compositions that are industrially relevant.

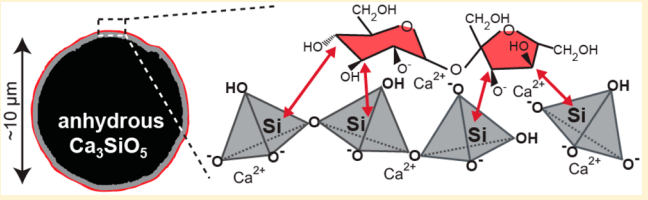

INTRODUCTION

Competitive adsorption of small quantities of organic species versus other chemical species (e.g., organic or inorganic species, water) at organic or inorganic surfaces can significantly influence dissolution, hydration, and crystallization processes in diverse synthetic and biogenic materials, especially those with low surface areas. For example, the growth rates and morphologies of molecular crystals can be controlled by using dilute chemical species that adsorb competitively at specific crystal facets or surface lattice sites.[1,2] Pathogenesis of kidney stones can be prevented by suppressing the undesirable growth of L-cystine by selective adsorption of architecturally similar molecules, such as L-cystine dimethylester, at fast-growing high-surface-energy crystal facets.[3] Saccharide and carboxylate moieties in small quantities have been shown to stabilize biogenic carbonates by controlling hydration and dissolution processes, thereby influencing the structures and mechanical properties of carbonate shells, spines, etc.[4−8] Furthermore, the adhesion of marine organisms, such as mussels, at hydrated inorganic surfaces is promoted by the interactions of saccharide species with Fe^{3+} cations.[9] Similar surface phenomena in calcium silicate and aluminate-based cementitious structural materials are strongly influenced by the presence of dilute concentrations of organic molecules in aqueous solutions. Generally, the molecular-level origins of the diverse adsorption behaviors of dilute organic species on low-surface-area solids are important to establish because they are often correlated with macroscopic rheological and mechanical properties.

In particular, the mechanical properties of aluminosilicate cements that enable their widespread structural applications develop through a series of steps involving dissolution,

Received: January 26, 2015
Published: June 1, 2015

DOI: 10.1021/jacs.5b00622
J. Am. Chem. Soc. 2015, 137, 8096−8112

precipitation, and crystallization of low-surface-area inorganic oxides (e.g., tricalcium silicate and tricalcium aluminate) in water.[10,11] Dilute concentrations (≤1% by weight of solids, bwos) of organic species are often used to slow the hydration kinetics and alter rheological properties[10,12−14] as desirable, for example, in oil well cementing operations that require fluidity of cement−water mixtures for extended times and at elevated pressures and temperatures. This involves competitive adsorption of organic molecules in place of water at silicate or aluminate particle surfaces, which slows or prevents the formation of hydration products. Despite their enormous technological importance, much remains unknown about the specific adsorption behaviors and molecular interactions of organic molecules at low-surface-area (ca. 1 m^2/g) silicate or aluminate particles. This is especially the case for dilute, industrially relevant concentrations (≤0.1% bwos) of adsorbate molecules, which are exceedingly difficult to detect and characterize at low bulk concentrations. These challenges are exacerbated by the heterogeneous molecular environments and lack of long-range structural order that are characteristic of surfaces in general and specifically in these complicated multicomponent solid−liquid mixtures.

The structures and compositions of hydrated silicate and aluminate species have been shown to depend strongly on the types and quantities of organic molecules used during hydration. Combined insights from characterization techniques, such as X-ray and neutron diffraction, infrared and Raman spectroscopy, X-ray absorption spectroscopy, and electron microscopy provide information over complementary length scales on the chemical transformations that occur as a result of hydration.[15] Such methods, however, provide limited insights on site-specific molecular-level interactions or adsorption behaviors of dilute chemical species at inorganic oxide surfaces. By comparison, nuclear magnetic resonance (NMR) spectroscopy methods are sensitive to local atomic environments and can be readily applied to solids lacking long-range structural order. For example, 1D solid-state ^{29}Si, ^{27}Al, and ^{43}Ca magic-angle-spinning (MAS) NMR measurements have been extensively used to monitor the transformation of silicate, aluminate, and calcium species, respectively, in cementitious materials hydrated without and with chemical additives (e.g., organic molecules).[11,16−22] Such 1D NMR methods, in combination with macroscopic calorimetry, conductivity, rheological, and compressive strength measurements, facilitate understanding of the effects of different organic compounds on the hydration rates of tricalcium silicate (Ca_3SiO_5) and more complicated cement mixtures.[12,14,21,23−27] Solid-state 2D $^{13}C\{^1H\}$, $^{29}Si\{^1H\}$, and $^{27}Al\{^1H\}$ heteronuclear correlation (HETCOR) and $^1H\{^1H\}$ double-quantum (DQ) NMR measurements of silicates and aluminates hydrated with organic additives (e.g., stabilizers or hydration inhibitors) have established surprisingly diverse influences of closely related organic molecules, such as glucose and sucrose, on the rates of hydration.[13,28,29] Similar 2D NMR methods have also been used to measure the molecular interactions of organic acids adsorbed at much higher concentrations (4−40% bwos) on titania and zirconia nanoparticles that also have high surface areas (50−150 m^2/g).[30] As conventionally practiced, however, NMR spectroscopy is relatively insensitive, so detecting and resolving the NMR signals from organic molecules and inorganic species in low-surface-area cementitious materials have required concentrations of at least 1% bwos of the organic species, which furthermore must often be isotopically enriched to be feasible.[13,26,28] Such relatively high loadings generally correspond to multilayers of organic molecules adsorbed on particle surfaces, and the bulklike characters of the multilayers tend to obscure the influences and interactions of the most-important first adsorption layer that is thought to be principally responsible for inhibiting hydration.

By comparison, industrially relevant concentrations are typically an order of magnitude lower (0.1% bwos) and correspond to approximately monolayer coverages of organic molecules on low-surface-area (∼1 m^2/g) particles. Such dilute loadings have been infeasible to characterize at a molecular level by conventional methods, including NMR. Nevertheless, recent advancements in dynamic-nuclear-polarization (DNP) NMR spectroscopy[31−34] have resulted in dramatically improved NMR signal sensitivity that opens new opportunities to probe the interactions of dilute quantities of surface-adsorbed organic species on low-surface-area solids. Solid-state DNP NMR techniques rely on continuous microwave irradiation to transfer the large electron spin polarization to nuclear spins. Dramatic NMR signal enhancements can result, up to a theoretical limit of the ratio of the electronic and nuclear gyromagnetic ratios ($\gamma_e/\gamma_H \sim 658$ for ^1H). These advances have enabled rapid acquisition of multidimensional NMR spectra for characterization of ^{13}C- and ^{15}N-labeled biological solids in frozen solutions where exogenous stable radicals are used as a source of electron polarization.[35−44] More recently, it has been shown that solid-state DNP surface-enhanced NMR spectroscopy (DNP SENS) can be used to selectively enhance NMR signals from nuclei present at surfaces in high-surface-area (500−1000 m^2/g) materials (e.g., surface-functionalized mesoporous silicas).[32,45] This DNP SENS approach has been demonstrated for ^{13}C and ^{29}Si moieties (at natural isotopic abundance) present at the surfaces of functionalized mesoporous silica nanoparticles[32,45] and subsequently applied to ^{13}C, ^{15}N, ^{17}O, ^{27}Al, ^{29}Si, and ^{119}Sn in a wide variety of relatively high-surface-area materials.[34,46−58] Here, DNP SENS measurements are shown to enable sensitive study of dilute (∼0.1% bwos) organic molecules adsorbed on low-surface-area (∼1 m^2/g) silicate particles and establish the molecular origins by which they inhibit hydration.

We hypothesize that the relative efficacies of surface-adsorbed organic molecules, such as saccharides and phosphonic acids, to inhibit silicate hydration are due to their molecular compositions and architectures, which directly influence their adsorption behaviors and chemistries in these complicated heterogeneous mixtures. Specifically, tricalcium silicate hydrated with dilute industrially relevant concentrations of sucrose, a representative nonreducing saccharide, and an industrially important organic compound, nitrilotri-(methylenephosphonic acid) (NTMP), are examined to establish how their different molecular structures (Chart 1) result in distinct surface interactions that dramatically inhibit hydration processes. High ^{13}C and ^{29}Si DNP NMR signal enhancements are reported here for low-surface-area (∼1 m^2/g) nonporous silicate particles with approximately monolayer coverages of surface-adsorbed organic molecules. This enables high-resolution solid-state 2D DNP NMR spectra of dilute surface species to be recorded in short measurement times (ca. 1 h) that are otherwise infeasible for these demanding material compositions using conventional NMR methods. To the best of our knowledge, this is the first time that such detailed molecular-level measurements have been reported on the surface chemistry of dilute species adsorbed on low-surface-area

DOI: 10.1021/jacs.5b00622
J. Am. Chem. Soc. 2015, 137, 8096−8112

Chart 1. Molecular Structural Formulas of Sucrose, Nitrilotri(methylenephosphonic acid), and bCTbK and TEKPol Biradicals

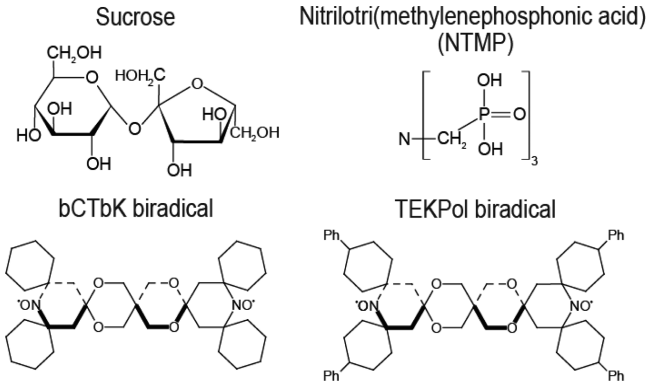

(~1 m^2/g) heterogeneous materials. The analyses yield detailed new understanding of the molecular compositions and site-specific interactions of organic moieties, hydroxyl species, water, and silicate species that account for the complicated influences of small amounts of surface-adsorbed molecules on the hydration behaviors of a technologically important silicate material.

MATERIALS AND METHODS

Anhydrous triclinic tricalcium silicate (Ca_3SiO_5, Mineral Research Processing, France), 99% ^{13}C-enriched D-sucrose ($C_{12}H_{22}O_{11}$, Sigma-Aldrich), and NTMP ($N(CH_2PO(OH)_2)_3$, Sigma-Aldrich, 10−20% impurity of aqueous inorganic acids) were used as received. Hydrated samples were prepared by mixing the anhydrous powders (approximately 500 mg) and hydration inhibitor (e.g., sucrose or NTMP) at a loading of 0.1% bwos with water in polyethylene containers using a vortex mixer (Fisher Scientific) at 3000 rpm for 2 min. Samples hydrated without inhibitors were prepared under otherwise identical conditions. The resulting mixtures were determined to have pH values of 12.7 (±0.1). Water-to-solids mass ratios of 0.50 were used for preparing samples of hydrated tricalcium silicate, which resemble typical industrial formulations. After mixing, all materials were allowed to hydrate for 4 h at 90 °C and 100% relative humidity, conditions that are similar to those used in oil well cementing applications. Following hydration, the products were immersed in liquid nitrogen and evacuated at 0.10 Torr and −40 °C to quench the hydration process and remove unreacted bulk or weakly adsorbed water by freeze-drying.[11] This method is expected to have negligible (if any) effects on the molecular-level chemistry of the hydrated samples and avoids the use of additional organic species that are often used in conventional techniques to quench hydration, which could complicate the analyses.[59] The solid samples of cementitious materials hydrated without or with hydration inhibitors were ground to a powder and kept dry thereafter in sealed vessels under vacuum to ensure no further molecular changes occurred in the samples prior to the DNP NMR measurements.

X-ray diffraction patterns were acquired on a Philips XPERT powder diffractometer using Cu Kα radiation with a wavelength of 1.54 Å. The samples were scanned at 12°/min between 2θ angles of 10−80° for tricalcium silicate hydrated (4 h, 90 °C) without (Figure 1a) and with (Figure 1b) 0.1% bwos ^{13}C-labeled sucrose. The reflections in Figure 1b are indexable to triclinic tricalcium silicate with the $P\bar{1}$ space group.[60] Figure 1a shows reflections that are indexable to calcium hydroxide ($Ca(OH)_2$) and calcium silicate hydrates, which partially overlap with the reflections indexable to tricalcium silicate.[10,61] Scanning electron micrographs were obtained using an FEI XL40 Sirion FEG digital scanning electron microscope at 15 000× magnification and 5 kV electron beam voltage for tricalcium silicate

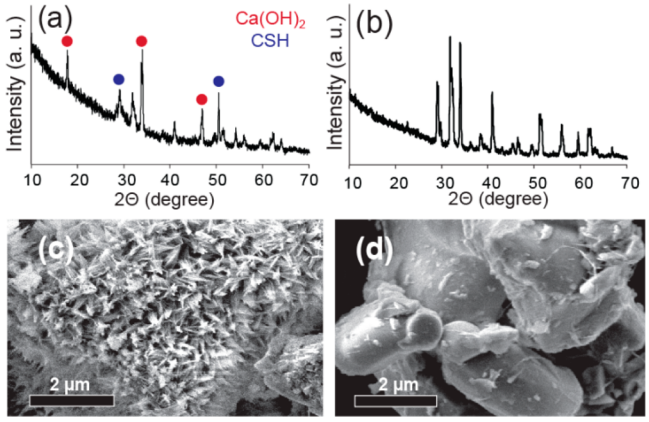

Figure 1. (a and b) Powder X-ray diffraction patterns and (c and d) SEM micrographs of hydrated tricalcium silicate (4 h, 90 °C) (a and c) without and (b and d) with 0.1% bwos ^{13}C-labeled sucrose. The principal indexable reflections corresponding to $Ca(OH)_2$ and calcium silicate hydrates are indicated in a. The reflections in b are indexable to the triclinic polymorph of tricalcium silicate. Calcium silicate hydrates (CSH), formed as the primary products of hydration in the absence of organic species, are observed on the surfaces of the particle in the SEM micrograph in c. In contrast, in the presence of 0.1% ^{13}C-labeled sucrose, no CSH are observed in the SEM micrograph in d.

hydrated (4 h, 90 °C) without and with 0.1% bwos ^{13}C-labeled sucrose and are shown in Figure 1c,d, respectively.

Solid-state NMR spectroscopy was used to characterize the molecular compositions and structures of hydrated cementitious materials. Conventional solid-state ^1H, ^{13}C, and ^{29}Si NMR experiments were conducted on an 11.7 T Bruker AVANCE-II NMR spectrometer, operating at frequencies of 499.84 MHz for ^1H, 125.69 MHz for ^{13}C, and 99.31 MHz for ^{29}Si, and under conditions of 10 kHz MAS at 25 °C using a Bruker 4 mm H-X double resonance probehead and zirconia rotors with Kel-F caps. (The natural abundances of the spin-1/2 ^1H, ^{13}C, ^{29}Si, and ^{31}P nuclei are 99.98, 1.1, 4.7, and 100%, respectively.) 1D single-pulse ^1H MAS spectra were acquired using a 90° pulse length of 4.0 μs and a recycle delay of 2 s. 1D single-pulse ^{29}Si MAS spectra were acquired using a 90° pulse length of 3.7 μs under conditions of proton decoupling (4.0 μs 90° ^1H pulses), and using a recycle delay of 500 s (5 × ^{29}Si spin−lattice relaxation time) to ensure thermal equilibration of the ^{29}Si magnetization between successive scans. ^{29}Si spin−lattice relaxation times (T_1) for the anhydrous and hydrated ^{29}Si silicate species were 97 (±12) and 76 (±4) s, respectively, as determined from ^{29}Si inversion−recovery measurements and analyses (Supporting Information, Figure S1). NMR line shape analyses were conducted using the software DMFit 2010,[62] with Gaussian or Lorentzian line shapes fit according to signal position, width, and amplitude. The ^1H, ^{13}C, and ^{29}Si NMR isotropic chemical shifts were referenced to tetramethylsilane, using tetrakis-(trimethylsilyl)silane [$((CH_3)_3Si)_4Si$] as a secondary standard, and ^{31}P NMR isotropic chemical shifts were referenced to a 85% phosphoric acid solution, using triphenylphosphine [$P(C_6H_5)_3$] as a secondary standard.[63,64]

Conventional solid-state cross-polarization (CP) MAS NMR experiments[65] involve the excitation of abundant nuclear spins (typically ^1H) and subsequent magnetization transfer via dipole−dipole couplings to dilute nuclear spins (e.g., ^{13}C, ^{29}Si, etc.), as depicted schematically by the pulse sequence in Figure 2a. In the DNP NMR experiments, continuous microwave irradiation at the electron paramagnetic resonance (EPR) frequency is incorporated into the conventional CPMAS experiment, as depicted in Figure 2b. Specifically, for nitroxide biradical polarizing agents, such as bis-cyclohexyl-TEMPO-bisketal (bCTbK) and TEKPol (Chart 1) used in this study, the DNP mechanism proceeds via the cross effect.[31,66,67] Previously, the majority of DNP NMR studies have been performed on analytes dispersed in frozen aqueous or nonaqueous solutions of

DOI: 10.1021/jacs.5b00622
J. Am. Chem. Soc. 2015, 137, 8096−8112

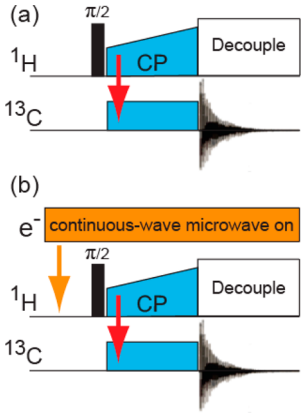

Figure 2. Schematic diagrams of solid-state 1D (a) $^{13}C\{^1H\}$ conventional CPMAS and (b) $^{13}C\{^1H\}$ DNP CPMAS experiments.

stable exogeneous paramagnetic centers.[67−70] By comparison, surface-enhanced DNP NMR experiments are most conveniently performed by incipient wetness impregnation of the solid powder samples with minimal volumes of a solution containing dissolved stable paramagnetic centers, usually a nitroxide biradical, to obtain a pastelike consistency.[32,34,45,66,67] This incipient wetness impregnation procedure brings the radical solution in contact with particle surfaces without significantly diluting the solid sample. Importantly, the CP step in the DNP NMR experiments ensures that only those moieties that are at the surface, and thus in close (<1 nm) molecular-level proximity to the ^1H spin reservoir, are hyperpolarized. Solid-state DNP SENS measurements were conducted on freeze-dried powder samples of hydrated cementitious materials impregnated with a nitroxide biradical (either bCTbK or TEKPol) dissolved in a suitable organic solvent.[47,66,67,71] Samples were prepared by combining approximately 30 mg of hydrated tricalcium silicate with 15−20 μL of a solution consisting of 2 or 4 mM bCTbK or TEKPol in 1,2-dichlorobenzene or 1,1,2,2-tetrachloroethane under conditions of incipient wetness at ambient temperature and pressure.[72] Each sample was mixed with a glass stirring rod to ensure macroscopically uniform distribution of the biradical solution over the solid powder sample. The resulting pastelike samples were packed into 3.2 mm sapphire MAS rotors and sealed with a polytetrafluoroethylene insert to prevent loss of solvent during the measurements. The rotor was capped with a zirconia drive cap and quickly inserted into the precooled DNP NMR probehead for measurements. Solid-state DNP SENS experiments were conducted on a Bruker 9.4 T AVANCE-III NMR spectrometer operating at frequencies of 399.95 MHz for ^1H, 100.57 MHz for ^{13}C, 79.46 MHz for ^{29}Si, and 161.90 MHz for ^{31}P, and under conditions of 8, 10, or 12.5 kHz MAS at 105 K. The spectrometer was equipped with a Bruker 3.2 mm H-X-Y triple resonance variable temperature MAS probe head, a cooling cabinet, and a 263 GHz gyroton microwave source and waveguide system.[73] 1D surface-enhanced $^{13}C\{^1H\}$ DNP NMR spectra were acquired using a 2 ms contact time, SPINAL-64 proton decoupling,[74] and a 2 s recycle delay. 2D $^{13}C\{^1H\}$ DNP HETCOR spectra were acquired under continuous microwave irradiation, using a 0.5 or 1.5 ms contact time, with 64 t_1 increments, an incremental step size of 32 or 64 μs, a recycle delay of 2 s, and 96 or 56 scans each. 2D $^{29}Si\{^1H\}$ DNP HETCOR spectra were acquired using a 3 ms contact time, with 64 t_1 increments, an incremental step size of 64 μs, a recycle delay of 3 s, and 32 or 128 scans each. 2D $^{31}P\{^1H\}$ DNP HETCOR spectra were acquired under continuous microwave irradiation, using a 1.5 ms contact time, with 48 t_1 increments, an incremental step size of 64 μs, a recycle delay of 3 s, and 4 scans each. All 2D DNP HETCOR spectra were acquired using eDUMBO-1_{22} homonuclear decoupling during the ^1H t_1 evolution period to enhance resolution in the ^1H dimension.[75] Solid-state 1D $^{29}Si\{^{13}C\}$ DNP REDOR[76] experiments were acquired using a 180° pulse length of 7.2 μs on ^{13}C to reintroduce the heteronuclear $^{29}Si-^{13}C$ dipolar couplings and a 3 s recycle delay. The uncertainties associated with the DNP REDOR data were estimated by the propagation-of-error method by using the signal-to-noise ratios of the spectra acquired without and with ^{13}C recoupling pulses.

RESULTS AND DISCUSSION

The hydration of tricalcium silicate is initiated at particle surfaces by the reaction of adsorbed water with surface silicate species in tricalcium silicate−water mixtures. Such reactions result in the transformation of anhydrous Q^0 silicate species to silanol Q^0 (nonhydrated) species that later partially cross-link to yield poorly ordered calcium silicate hydrates consisting of (hydrated) Q^1 and Q^2 silicate species.[77] (Q^n refers to silicon atoms that are covalently bonded via bridging oxygen atoms to $0 \leq n \leq 4$ other silicon atoms.)[78] The formation of such partially cross-linked silicate hydration products is responsible for cement setting and solidification in commercial cement−water mixtures, where tricalcium silicate is typically the major solid component (50−70 wt %). The hydration processes are strongly suppressed in the presence of dilute quantities of adsorbed sucrose or NTMP molecules, though the compositions and molecular architectures of these compounds are very different. 1D and 2D solid-state NMR methods, including surface-enhanced DNP NMR techniques, allow dilute surface species to be detected, relative quantities of distinct silicate species to be estimated, and intermolecular interactions between different silicate species, organic molecules, and water to be established.

Saccharide-Mediated Hydration of Tricalcium Silicate. *Quantification of Silicate Species in Hydrated Tricalcium Silicate.* Low absolute concentrations of organic compounds, such as saccharides or phosphonic acids, can strongly inhibit silicate hydration, which is attributed to their favorable adsorption properties compared to water at silicate particle surfaces. To understand the effects of dilute organic species on surface hydration processes, it is important to establish the molecular compositions and mutual interactions of water, silicate species, and organic molecules at the particle surfaces and to distinguish between sorption at nonhydrated and hydrated surfaces. Sucrose is a nonreducing disaccharide with furanose and pyranose rings that are covalently bonded through an $\alpha-\beta$ glycosidic linkage (Chart 1), which imparts distinct structural relationships among the different hydroxyl and proton moieties within a given molecule that have important implications for how sucrose adsorbs at oxide surfaces. Specifically, the adsorption of sucrose molecules at tricalcium silicate particle or hydration product surfaces inhibits the hydration of anhydrous silicate species to form calcium silicate hydrates.[13] The different types of silicate species can be identified and quantified by using solid-state ^{29}Si NMR measurements and thereby establish the molecular silicate structures and compositions after hydration without and with the presence of dilute quantities (0.1% bwos) of sucrose. For example, the 1D single-pulse ^{29}Si MAS spectrum of hydrated tricalcium silicate (4 h, 90 °C) in Figure 3a shows resolved ^{29}Si signals from distinct anhydrous and hydrated silicate species. Specifically, the spectrum exhibits eight narrow (<0.1 ppm full-width-half-maximum, fwhm) ^{29}Si signals in the range of −68 to −75 ppm from anhydrous Q^0 silicate species that primarily comprise the bulk of the low-surface-area (ca. 1 m^2/g) silicate particles.[78] The eight ^{29}Si signals correspond to nine distinct crystallographic sites in triclinic tricalcium silicate, previously established by diffraction measurements,[60,79] where two ^{29}Si sites have similar ^{29}Si atomic environments and chemical shifts

DOI: 10.1021/jacs.5b00622
J. Am. Chem. Soc. 2015, 137, 8096−8112

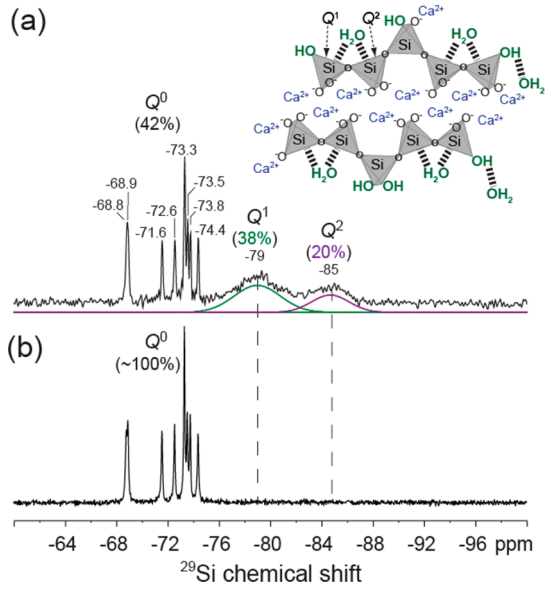

Figure 3. Solid-state 1D single-pulse ^{29}Si MAS NMR spectra of hydrated tricalcium silicate (4 h, 90 °C) (a) without and (b) with 0.1% bwos ^{13}C-labeled sucrose acquired at 11.7 T, 25 °C, and 10 kHz MAS. Inset in a shows a schematic representation of the different cross-linked four-coordinate Q^1 and Q^2 ^{29}Si moieties in calcium silicate hydrates, which are the primary products of silicate hydration.

(at −73.3 ppm and twice the signal intensity of the other signals) that are not resolved. Upon hydration, the anhydrous Q^0 silicate species are partially cross-linked to form calcium silicate hydrates, which result in the ^{29}Si signals at −79 ppm (Q^1) and −85 ppm (Q^2) in the ^{29}Si MAS spectrum. Compared to the ^{29}Si signals from anhydrous Q^0 species, the ^{29}Si signals from the Q^1 and Q^2 species are relatively broad (~4 ppm, fwhm) indicating distributions of local atomic environments for such hydrated silicate species, which are consistent with the poorly ordered character of calcium silicate hydrates. The inset in Figure 3a shows a schematic diagram of the different silicate species that are present in the calcium silicate hydrates, consistent with previous ^{29}Si NMR results,[11,13] diffraction measurements,[80,81] and theoretical calculations.[77,82] The extent of silicate hydration is estimated by comparing the relative integrated intensities of the ^{29}Si signals associated with Q^0 (42%), Q^1 (38%), and Q^2 (20%) silicate species in the ^{29}Si MAS spectrum. Approximately 58% of the silicate species have therefore converted to calcium silicate hydrates under these hydration conditions in the absence of sucrose. Comparison of the relative intensities of the eight distinct ^{29}Si signals from anhydrous Q^0 ^{29}Si species furthermore establish that there is no preferential reaction of any of the anhydrous silicate sites with water during the hydration process.

By comparison, in the presence of dilute quantities (0.1% bwos) of sucrose, no measurable amounts of calcium silicate hydrates are observed by conventional NMR (or other) techniques, which indicates that a small amount of sucrose strongly inhibits silicate hydration processes. Similar analysis of the 1D single-pulse ^{29}Si MAS spectrum of tricalcium silicate hydrated under otherwise identical conditions, except for the presence of 0.1% bwos sucrose (Figure 3b), reveals no detectable ^{29}Si signals from the Q^1 and Q^2 species associated with the silicate hydration products. This establishes that there is no significant conversion of anhydrous Q^0 silicate species to calcium silicate hydrates in the presence of 0.1% bwos sucrose within the sensitivity limits of the conventional solid-state NMR experiment. The atomic-level NMR results are manifested macroscopically at micrometer length scales by morphological differences between tricalcium silicate hydrated without and with 0.1% bwos sucrose, as seen in the scanning electron micrographs (SEM) shown in Figure 1c,d, respectively. In the absence of sucrose, tricalcium silicate reacts with water to yield calcium silicate hydrates that are observed in the electron micrograph (Figure 1c) as needlelike structures on the particle surfaces. By comparison, the electron micrograph (Figure 1d) of tricalcium silicate hydrated in the presence of 0.1% bwos sucrose reveals almost exclusively bulk anhydrous silicate particles with little or no detectable products of hydration. The molecular-level NMR and micrometer-scale SEM results clearly establish that tricalcium silicate hydration is strongly inhibited by the presence of dilute sucrose concentrations (0.1% bwos), which approximately correspond to monolayer coverages (analysis in Supporting Information) of the low-surface-area (~1 m^2/g) silicate particles by sucrose molecules.

Previous studies of silicate hydration in the presence of high and industrially unrealistic loadings of sucrose (ca. 1% bwos on similar ~1 m^2/g particles)[13,26,28,83] correspond to multilayered adsorption that may obscure the crucial role of the molecules adsorbed directly at the silicate particle or hydration product surfaces. Furthermore, the excess multilayers represent an additional possible diffusion barrier to water that is absent under industrially relevant compositions. In contrast, the SEM and quantitative ^{29}Si NMR results in Figures 1 and 3, respectively, provide morphological and molecular-level evidence that significantly lower loadings of sucrose effectively inhibit surface hydration. However, these measurements have insufficient sensitivity and resolution to determine the molecular origins of such surface chemistry effects, which could include competitive adsorption of organic molecules in place of water at either nonhydrated species to inhibit nucleation of calcium silicate hydrates or on early-stage hydration products to inhibit subsequent growth.

Identification of Dilute Saccharide Surface Species. Measuring the crucial molecular interactions of surface-adsorbed sucrose monolayers has previously been infeasible because of the low signal sensitivity of conventional solid-state NMR methods. By comparison, solid-state surface-enhanced DNP NMR techniques[32,34,45] provide significantly enhanced signal sensitivity that enables the detection of dilute species, including surface-adsorbed sucrose molecules. To conduct such measurements, powdered samples were combined with minimal volumes of a 1,2-dichlorobenzene solution containing dissolved stable nitroxide biradicals under incipient wetness conditions and quickly (<10 min) introduced into the precooled DNP NMR probehead.[32,34,45,66,67] 1,2-Dichlorobenzene was selected for its hydrophobic properties that are expected to perturb minimally the interactions between sucrose, water, and surface silicate species, all of which are hydrophilic. (Additionally, the ^{13}C signals of 1,2-dichlorobenzene and sucrose do not overlap.) The DNP NMR experiments use continuous microwave irradiation at ca. 100 K to transfer high electron spin polarization (from stable biradicals, such as bCTbK or TEKPol) via hyperfine interactions to ^{1}H nuclei of the frozen 1,2-dichlorobenzene DNP solvent molecules and adsorbed sucrose, as shown in the schematic diagram in Figure 4. The DNP-enhanced ^{1}H spin polarization is subsequently distributed by ^{1}H−^{1}H spin diffusion to other ^{1}H nuclei of molecularly proximate (<1 nm) solvent molecules and to the

DOI: 10.1021/jacs.5b00622
J. Am. Chem. Soc. 2015, 137, 8096−8112

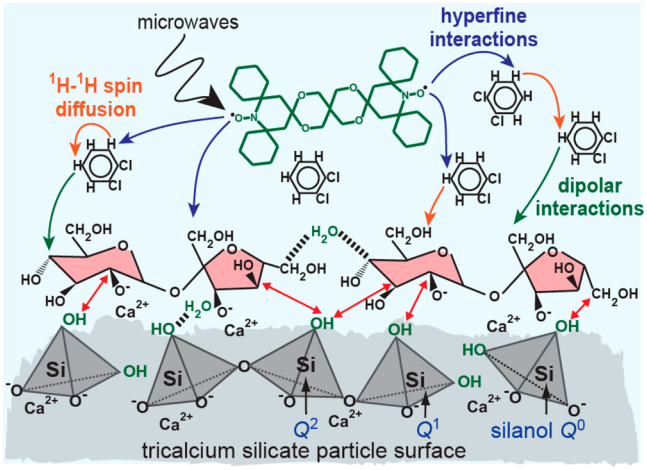

Figure 4. Schematic diagram depicting the adsorption of sucrose molecules at silicate particle surfaces and the various polarization transfer pathways involved in the dynamic nuclear polarization (DNP) NMR experiments, including DNP (blue) from electrons to ^{1}H nuclei through hyperfine interactions, ^{1}H−^{1}H spin diffusion (orange), and cross-polarization (CP, green) from ^{1}H to dilute nuclei (e.g., ^{13}C and ^{29}Si) through dipolar interactions. The nitroxide biradical polarizing agent shown is bCTbK.

silicate particle surfaces, though importantly, not to their dense nonhydrated interiors. Subsequently, cross-polarization (CP)[65] is used to transfer the DNP-enhanced polarization of ^{1}H nuclei to dilute spins (i.e., ^{29}Si and ^{13}C), including those present in surface silicate species and adsorbed sucrose molecules. Figure 5a shows the 1D ^{13}C{^{1}H} DNP CPMAS spectrum (red) acquired with microwave irradiation of tricalcium silicate hydrated (4 h, 90 °C) with 0.1% bwos ^{13}C-labeled sucrose that exhibits intense and well-resolved ^{13}C signals in the range of 50−100 ppm from the chemically distinct ^{13}C sites in surface-adsorbed sucrose molecules.[28] The enhanced ^{13}C signal intensity demonstrates marked improvement in signal sensitivity compared to that of conventional solid-state NMR methods, as exemplified by the 1D ^{13}C{^{1}H} CPMAS spectrum (Figure 5a, black) acquired on the same sample and under otherwise identical conditions but without microwave irradiation. The DNP NMR signal enhancement (ε) is quantified as the ratio of the ^{13}C signal intensities obtained with and without microwave irradiation for the different resolved ^{13}C signals, which for sucrose was measured to be $\varepsilon_{C-sucrose}$ = 12. A similar DNP enhancement ($\varepsilon_{C-solvent}$ = 18; Supporting Information, Figure S2) was observed for the ^{13}C signal at 130 ppm associated with the 1,2-dichlorobenzene DNP solvent. Interestingly, such improved signal sensitivity also enables the detection of a ^{13}C signal at 170 ppm (Figure 5a, red), which is attributed to small quantities of calcium carbonate species ($CaCO_3$)[84] resulting from dissolution of atmospheric carbon dioxide and reaction with water near tricalcium silicate particle surfaces.[10] The concentration of biradical species significantly influences the DNP NMR signal enhancements that are obtained as shown in Figure 5b, where the ^{13}C and ^{29}Si DNP NMR signal enhancements are plotted as functions of bCTbK (nitroxide biradical) concentration. The characteristic trend observed in the graph is similar to that observed previously for homogeneous solutions containing biradical polarizing agents[85,86] and high-surface-area solids wetted with radical solutions:[32,47] Signal enhancements increase initially with biradical concentration and exhibit a maximum, before

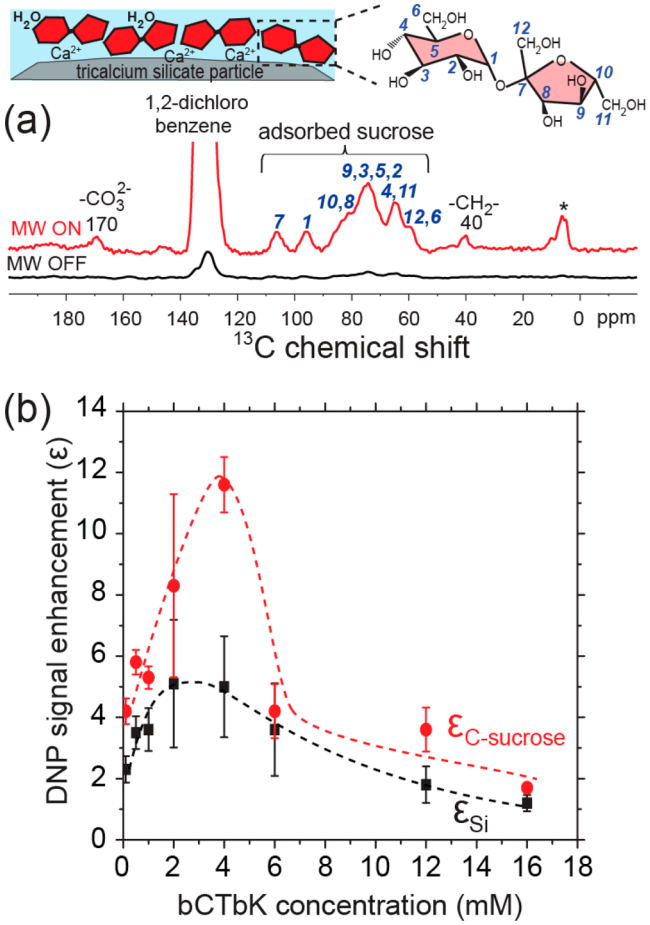

Figure 5. (a) Solid-state surface-enhanced 1D ^{13}C{^{1}H} DNP CPMAS spectra of hydrated tricalcium silicate (4 h, 90 °C) with 0.1% bwos ^{13}C-labeled sucrose. The spectra were acquired in the presence of 4 mM bCTbK in frozen 1,2-dichlorobenzene, at 9.4 T, 105 K, 12.5 kHz MAS, and (black) without or (red) with microwave irradiation at 263 GHz, the latter of which was recorded in 9 min (256 scans). The ^{13}C DNP NMR signal enhancement for ^{13}C signals from adsorbed sucrose species ($\varepsilon_{C-sucrose}$) was determined to be approximately 12. The asterisk indicates a MAS sideband from the frozen solvent.[87] The schematic inset in a depicts the monolayer coverage of silicate particles by adsorbed sucrose molecules, along with a structural representation of sucrose with the carbon atoms labeled. (b) Experimentally measured ^{13}C and ^{29}Si DNP NMR signal enhancements for surface species are shown in red and black, respectively, as functions of the bulk solution concentration of bCTbK (biradical) in the frozen 1,2-dichlorobenzene DNP solvent. DNP NMR signal enhancements are estimated as the ratio of the signal intensities with and without microwave irradiation for specific NMR signals.

decreasing as a result of increased paramagnetic broadening or shorter spin−lattice relaxation times. However, for the latter, maximum DNP NMR signal enhancements are typically achieved at relatively high biradical concentrations (16−20 mM). In contrast, the maximum DNP NMR signal enhancement is obtained here at a substantially lower biradical concentration of 4 mM because of the significantly lower mean surface area of the silicate particles. Surface-enhanced ^{13}C{^{1}H} DNP CPMAS measurements conducted using the optimum biradical concentration (4 mM) enable dilute (0.1% bwos) surface-adsorbed sucrose molecules to be detected in unprecedentedly short times (9 min for the ^{13}C{^{1}H} DNP

DOI: 10.1021/jacs.5b00622
J. Am. Chem. Soc. 2015, 137, 8096−8112

CPMAS spectrum in Figure 5a, red) and without significant loss of spectral resolution.

The presence of biradical and solvent species, as required for the DNP NMR measurements, do not detrimentally affect the surface compositions at particle surfaces. This can be elucidated by comparing the surface-enhanced $^{13}C\{^1H\}$ DNP CPMAS spectrum of tricalcium silicate hydrated in the presence of 0.1% bwos ^{13}C-sucrose (Figure 5a, red) with a conventional $^{13}C\{^1H\}$ CPMAS spectrum of tricalcium silicate hydrated in the presence of 1% bwos ^{13}C-sucrose (Supporting Information, Figure S3). Both spectra exhibit ^{13}C signals between 50 and 100 ppm with similar ^{13}C isotropic chemical shifts and line shapes, establishing that the introduction of exogeneous paramagnetic species (bCTbK) and organic solvent (1,2-dichlorobenzene) appears not to alter or modify significantly the compositions and structures of the organic surface species.[87] These results, in combination with separate solution- and solid-state ^{13}C NMR measurements (Supporting Information, Figure S4), point to negligible dissolution or reaction of the sucrose moieties of interest with bCTbK biradical or 1,2-dichlorobenzene solvent species.[88] Importantly, signals from ^{13}C species in adsorbed monolayers of sucrose molecules (corresponding to 0.1% bwos) can be rapidly detected and measured by surface-enhanced DNP NMR measurements. Comparison of the measurement times associated with the 1D $^{13}C\{^1H\}$ CPMAS spectra of tricalcium silicate hydrated with 1% bwos (acquired without DNP in 68 min, 2048 scans) and 0.1% bwos (acquired with DNP in 9 min, 256 scans) ^{13}C-sucrose demonstrate the enormous improvement in NMR signal sensitivity and similarly dramatic reduction in measurement time. Such enhanced signal sensitivity represents a breakthrough in the capability to detect and identify dilute molecular species on low-surface-area silicate particles, which were previously infeasible by using conventional NMR or other methods.

Adsorption Interactions of Sucrose at Heterogeneous Silicate Particle Surfaces. Detailed insights on silicate surface chemistry, such as the types, structures, and relative distributions of silicate species, can be combined with structural details of the adsorbed sucrose molecules to probe their adsorption behaviors at specific sites on the particle surfaces. The quantitative 1D single-pulse ^{29}Si MAS spectrum of tricalcium silicate hydrated with 0.1% bwos sucrose (Figure 6a) exhibits no detectable ^{29}Si signal intensity at −79 and −85 ppm associated with hydrated Q^1 and Q^2 species in calcium silicate hydrates, as previously discussed. A conventional 1D $^{29}Si\{^1H\}$ CPMAS spectrum of the same material (Figure 6b) exhibits at least two inhomogeneously broadened ^{29}Si signals centered at −73 and −79 ppm that correspond to silanol Q^0 and hydrated Q^1 silicate species, respectively, which are present in close (<1 nm) molecular proximity to ^1H species at the particle surfaces. Silanol Q^0 species are monomeric silicate moieties that are present at tricalcium silicate surface sites and can be associated with different numbers of hydroxyl groups (e.g., $Si(OH)_3O^-$ or $Si(OH)_4$). Recent theoretical and experimental studies have suggested that such silanol Q^0 surface species transform to yield partially cross-linked Q^1 and Q^2 species associated with calcium silicate hydrates.[89−92] Detection of 1D ^{29}Si signals from such surface species required extensive signal averaging (24 h), consistent with their very dilute concentrations. The results establish that even in the presence of low concentrations of adsorbed sucrose molecules

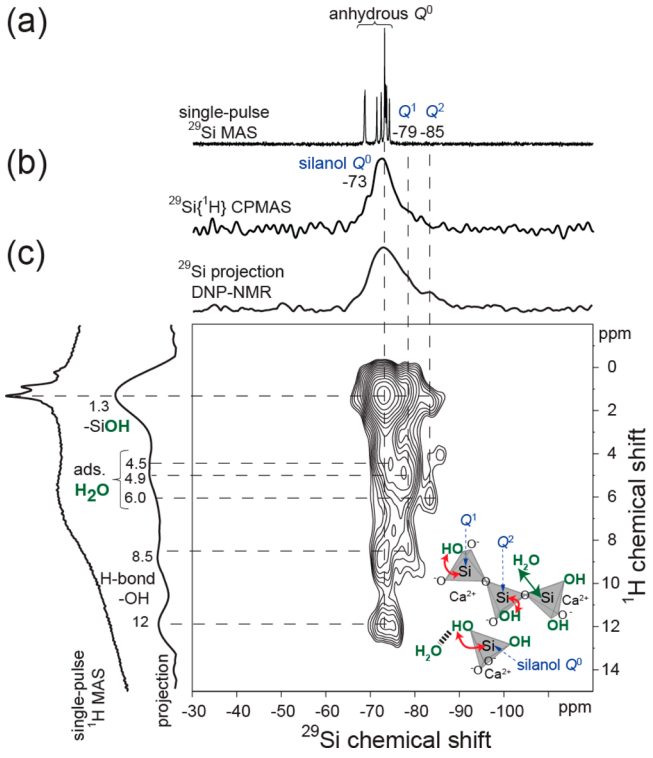

Figure 6. Solid-state (a) 1D single-pulse ^{29}Si MAS, (b) 1D $^{29}Si\{^1H\}$ CPMAS, and (c) 2D surface-enhanced $^{29}Si\{^1H\}$ DNP HETCOR spectra of hydrated tricalcium silicate (4 h, 90 °C) with 0.1% bwos ^{13}C-labeled sucrose (same sample as in Figure 3b). The spectra in a and b were acquired at 11.7 T, 25 °C, and 10 kHz MAS. The 2D spectrum in c was acquired with 4 mM TEKPol (biradical) in frozen 1,2-dichlorobenzene (the DNP solvent), with continuous microwave irradiation at 263 GHz, at 9.4 T, 105 K, and 12.5 kHz MAS. The spectra were recorded in total experimental times of (a) 14 h, (b) 24 h, and (c) 1.4 h. The inset in c shows a schematic diagram of silanol Q^0 and cross-linked Q^1 and Q^2 ^{29}Si species in tricalcium silicate hydration products present at particle surfaces, along with their molecular and dipolar interactions with −SiOH species (red arrows) and adsorbed water (green arrow). A 1D single-pulse ^1H MAS spectrum acquired at 11.7 T, 25 °C, and 10 kHz MAS is shown along the vertical axis in c for comparison with the 1D projection of the 2D spectrum. The numbers above or alongside the NMR signals indicate their corresponding isotropic chemical shifts.

small quantities of silanol Q^0 species as well as calcium silicate hydrates are present at the particle surfaces. Although the 1D NMR measurements yield the types and relative quantities of organic and silicate molecular species present in the silicate−water−adsorbate mixtures, they provide little information on specific molecular interactions or on the distributions of the different chemical species.

The molecular-level surface interactions that account for the adsorption properties of organic molecules at silicate surfaces are expected to aid understanding of their influences on the hydration processes. Such insights can be established by using solid-state 2D surface-enhanced DNP NMR measurements, which can be recorded within feasible measurement times (e.g., hours) and with high resolution. Specifically, 2D $^{29}Si\{^1H\}$ and $^{13}C\{^1H\}$ DNP HETCOR experiments can be used to measure and identify the key molecular interactions between adsorbed saccharide species, water, and silicate species by correlating their respective isotropic chemical shifts, even for dilute monolayer coverages on low-surface-area particles. For

DOI: 10.1021/jacs.5b00622
J. Am. Chem. Soc. 2015, 137, 8096−8112

example, 2D ^{29}Si{^{1}H} DNP HETCOR methods selectively detect those ^{29}Si nuclei that are dipole−dipole-coupled to ^{1}H nuclei from moieties that are in molecular-level (<1 nm) proximity. The resulting 2D intensity correlations establish site-specific interactions between ^{29}Si and ^{1}H nuclei, including those associated with silanol moieties (−SiOH) and adsorbed water, which are present at the hydrating particle surfaces. Figure 6c shows the solid-state 2D ^{29}Si{^{1}H} DNP HETCOR spectrum of tricalcium silicate hydrated (4 h, 90 °C) in the presence of 0.1% bwos ^{13}C-labeled sucrose that provides improved signal sensitivity and ^{1}H resolution (compared to the single-pulse ^{1}H MAS spectrum in Figure 6c, left). Strong correlated intensity is resolved between ^{29}Si signals at −73, −79, and −85 ppm from silanol Q^0, hydrated Q^1 and Q^2 species, respectively, and the ^{1}H signal at 1.3 ppm from hydroxyl moieties (−SiOH) bonded to silanol Q^0 or hydrated silicate species (as depicted in the accompanying schematic diagram). The spectrum also exhibits correlated intensity between the same ^{29}Si signals at −73, −79, and −85 ppm and distinct signals at 4.5, 4.9, and 6.0 ppm, respectively, in the ^{1}H dimension, which are attributed to water in distinct molecular environments. This is consistent with recent theoretical studies that have proposed the presence of local structural differences in water present in the disordered calcium silicate hydrates, for which no molecular-level experimental evidence has previously been established.[82,93] Additional 2D intensity correlations are observed between the ^{29}Si signal at −73 ppm and ^{1}H signals at 8.5 and 12 ppm that arise from hydrogen-bonded −OH species present near silanol Q^0 surface sites. Similar correlated intensity is partially resolved between the ^{29}Si signal at −79 ppm from hydrated Q^1 species and the ^{1}H signal at 8.5 ppm from hydrogen-bonded −OH moieties. The ^{1}H signal assignments for the distinct −SiOH moieties and water are based on previous NMR studies of silicas, silicates, aluminosilicates, and calcium silicate hydrates.[11,13,28,78,94−97] Notably, the 2D spectrum shows no detectable correlated intensity between the ^{29}Si signal at −85 ppm (Q^2 species) and ^{1}H signals from hydrogen-bonded −OH moieties (between 8 and 12 ppm), consistent with their fewer nonbridging oxygen atoms (two for Q^2 compared to three for Q^1 species) and fewer hydrogen bonds. This is corroborated by recent molecular simulations that indicate the presence of different extents of hydrogen bonding among oxygen atoms on distinct four-coordinate silicate species (e.g., Q^1 and Q^2) and water molecules present in confined nanopores in calcium silicate hydrates.[93] These studies propose that the water molecules form hydrogen bonds with other water molecules and both bridging and nonbridging oxygen atoms in the calcium silicate hydrates. Furthermore, the simulations suggest that the strongest hydrogen bonds are formed with the nonbridging oxygen atoms, for which the NMR results presented here provide direct experimental evidence.

The surface hydration products formed in the presence of sucrose exhibit similar molecular-level structures as present in fully hydrated bulk products (e.g., in the absence of sucrose), despite their markedly different extents of silicate hydration. This is elucidated by comparing the 2D ^{29}Si{^{1}H} HETCOR spectra of tricalcium silicate hydrated (4 h, 90 °C) without sucrose (acquired without DNP, Supporting Information, Figure S5) and with 0.1% bwos sucrose (acquired with DNP, Figure 6c). Importantly, such comparisons also establish that the treatment of the solid samples as required for the solid-state DNP NMR measurements does not chemically alter the molecular structures, speciation, or interactions in partially hydrated tricalcium silicate.

Sucrose molecules competitively adsorb at surface silanol Q^0 and hydrated silicate sites to inhibit hydration reactions. Specific interactions between surface silicate species and adsorbed sucrose molecules can be probed by complementary solid-state 2D ^{13}C{^{1}H} DNP HETCOR measurements of tricalcium silicate hydrated in the presence of 0.1% bwos ^{13}C-labeled sucrose. Such measurements can be used to detect and correlate isotropic chemical shifts of signals associated with dipole−dipole-coupled ^{13}C and ^{1}H nuclear spins in chemical moieties. For example, the 2D ^{13}C{^{1}H} DNP HETCOR spectrum in Figure 7a of hydrated tricalcium silicate (4 h, 90 °C) in the presence of 0.1% bwos ^{13}C-labeled sucrose, acquired with a short CP contact time (0.5 ms), enables the detection and identification of ^{1}H species, according to the different organic ^{13}C-sucrose moieties with which they interact at silicate particle surfaces. (Supporting Information Figure S6 shows the 2D ^{13}C{^{1}H} DNP HETCOR spectrum presented over a wide ^{13}C chemical shift range to also show the ^{13}C signals from the DNP solvent species.) Strong correlated intensity is observed in the 2D ^{13}C{^{1}H} DNP HETCOR spectrum corresponding to intramolecular dipolar interactions between all of the ^{13}C-sucrose signals and the ^{1}H signal at 4.3 ppm from −CH and −COH moieties in the sucrose molecules.[28] Additional intensity correlations are observed between ^{13}C signals at 59 ppm (carbon atoms 12 and 6), 64 ppm (carbon atoms 4 and 11), 73 ppm (carbon atoms 9, 3, 5, and 2), and 81 ppm (carbon atoms 10 and 8) and the ^{1}H signal at 9.4 ppm that corresponds to hydrogen-bonded −OH species in close proximity to saccharide molecules near or at the silicate surfaces. Here, use of the short CP contact time (0.5 ms) allows identification of only the most strongly dipole−dipole-coupled ^{13}C and ^{1}H species that are associated with intramolecular interactions, thereby allowing their signals to be assigned confidently.

More importantly, 2D intensity correlations corresponding to intermolecular interactions are resolved in the 2D ^{13}C{^{1}H} DNP HETCOR spectrum (Figure 7b) of the same sample acquired with a longer CP contact time (1.5 ms). These are characterized by weaker dipole−dipole interactions (more distant moieties). As for the spectrum acquired with a short CP contact time, strong correlated intensity is also observed in the spectrum acquired with the longer CP contact time between all the ^{13}C signals from sucrose and the ^{1}H signal at 4.3 ppm from −CH and −COH moieties. Interestingly, the 2D ^{13}C{^{1}H} DNP HETCOR spectrum (Figure 7b) reveals strong intermolecular intensity correlations between sucrose ^{13}C signals at 59 ppm (12 and 6), 64 ppm (4 and 11), and 73 ppm (9, 3, 5, and 2) and the ^{1}H signal at 6.3 ppm that corresponds to water in close proximity to the sucrose molecules. In conjunction with the 2D ^{29}Si{^{1}H} DNP HETCOR NMR results in Figure 6c, such coadsorbed water molecules in the presence of sucrose appear not to promote the formation of Q^1 and Q^2 silicate hydration products. This suggests that although competitive adsorption of sucrose does not completely displace water molecules from the particle surfaces, hydration reactions are effectively inhibited, if not entirely halted. Correlated intensity is also resolved in the spectrum between sucrose ^{13}C signals at 59 ppm (12 and 6), 64 ppm (4 and 11), 73 ppm (9, 3, 5, and 2), and 81 ppm (10 and 8) and the ^{1}H signal centered at 1.3 ppm from hydroxyl moieties (−SiOH) associated with silanol Q^0 and hydrated Q^1 and Q^2 species, as assigned in the 2D ^{29}Si{^{1}H} DNP HETCOR

DOI: 10.1021/jacs.5b00622
J. Am. Chem. Soc. 2015, 137, 8096−8112

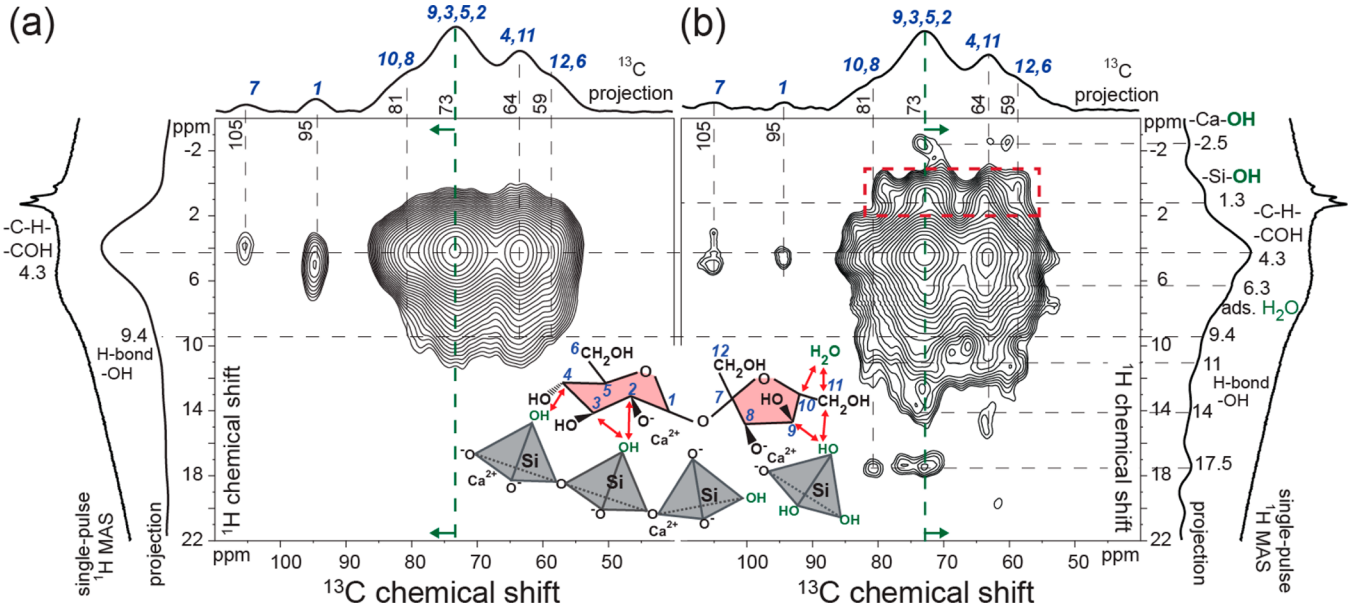

Figure 7. Solid-state surface-enhanced 2D ^{13}C{^{1}H} DNP HETCOR spectra of hydrated tricalcium silicate (4 h, 90 °C) with 0.1% bwos ^{13}C-labeled sucrose acquired with different contact times of (a) 0.5 ms and (b) 1.5 ms. The 2D spectra were acquired with 4 mM bCTbK (biradical) in frozen 1,2-dichlorobenzene (the DNP solvent), with continuous microwave irradiation at 263 GHz, at 9.4 T, 105 K, and 12.5 kHz MAS. The measurement times for the 2D spectra were (a) 3.4 h and (b) 2 h. Quantitative 1D single-pulse ^{1}H MAS NMR spectra acquired at 11.7 T, 25 °C, and 10 kHz MAS are shown along the vertical axes for comparison with the 1D projections of the 2D spectra. The inset shows a schematic diagram depicting the various chemical species and intermolecular interactions (red arrows) established by intensity correlations in the 2D spectra. The isotropic chemical shifts of ^{1}H species (vertical axes) are labeled alongside their respective NMR signals in a and b. The numbers above the ^{13}C signals (horizontal axes in a and b) indicate the respective ^{13}C sucrose moiety to which they are assigned, as labeled in the schematic structure of sucrose shown in the inset.

spectrum of Figure 6c. These intensity correlations (highlighted by a red, dotted-line rectangle in Figure 7b) unambiguously establish that ^{13}C sucrose moieties interact with isolated −SiOH moieties associated with silanol Q^0 and hydrated silicate surface species that are in close (<1 nm) molecular proximities, as depicted in the accompanying schematic diagram. Previous studies[98] of sucrose in alkaline solutions have indicated that partially deprotonated carbinol groups interact electrostatically with Ca^{2+} cations. Under the highly alkaline conditions used here, similar electrostatic interactions are expected to occur between partially deprotonated carbinol moieties in the sucrose molecules and surface Ca^{2+} cations. Therefore, Ca^{2+} cations near isolated −SiOH species are expected to mediate the adsorption of sucrose at Ca_3SiO_5 particle surfaces.

In addition, hydrogen-bonding interactions between −SiOH surface species and carbinol sucrose moieties contribute importantly to the competitive adsorption of sucrose in place of water at tricalcium silicate particle surfaces. Partially resolved 2D intensity is notably observed in the 2D ^{13}C{^{1}H} DNP HETCOR spectrum (Figure 7b) between sucrose ^{13}C carbinol signals centered at 59 ppm (12 and 6), 64 ppm (4 and 11), 73 ppm (9, 3, 5, and 2), and 81 ppm (10 and 8) and the ^{1}H signals at 9.4 and 11 ppm from hydrogen-bonded −OH species, consistent with the 2D spectrum acquired using short CP contact time (Figure 7a). Intermolecular interactions are also associated with the intensity correlations between signals at 14 and 17.5 ppm in the ^{1}H dimension from hydrogen-bonded −OH species and signals at 64 ppm (4 and 11) and 73 ppm (9, 3, 5, and 2) in the ^{13}C dimension that correspond to carbinol groups of adsorbed sucrose molecules. These intensity correlations indicate that sucrose adsorption is mediated by hydrogen-bonding between sucrose carbinol moieties and −SiOH groups at particle surfaces. Yesinowski et al. have noted that the isotropic ^{1}H chemical shifts of hydrogen-bonded species associated with similar mineral silicates are approximately inversely proportional to the lengths of their hydrogen bonds.[99] In the 2D ^{13}C{^{1}H} DNP HETCOR spectrum (Figure 7b), strongly hydrogen-bonded species associated with short hydrogen bond lengths correspond to ^{1}H signals at >9 ppm, compared to weakly hydrogen-bonded or isolated −SiOH species that are manifested by ^{1}H signals at ca. 1.3 ppm. The broad intensity correlations between ^{13}C signals at 59, 64, 73, and 81 ppm and ^{1}H signals at >9 ppm indicate a distribution of strongly hydrogen-bonded surface species, which is consistent with a distribution of local molecular environments for sucrose adsorbed on the heterogeneous surfaces of partially hydrated tricalcium silicate.

It is also interesting to note evidence for sucrose interactions with nanoscale solid byproducts of silicate hydration. Weak intensity correlations are observed between the ^{13}C signals at ca. 60 ppm (4, 11, 12, and 6) and 73 ppm (9, 3, 5, and 2) from sucrose and the ^{1}H signal at −2.5 ppm attributed to −CaOH moieties that are associated with calcium hydroxide (portlandite, $Ca(OH)_2$), a common byproduct of tricalcium silicate hydration). Similar −CaOH moieties have previously been observed in hydrated tricalcium silicate−water mixtures and calcium hydroxide using solid-state ^{1}H NMR measurements.[52,100] However, no indexable reflections from $Ca(OH)_2$ are detected in the X-ray diffraction pattern (Figure 1b) of the material. This indicates that these $Ca(OH)_2$ species likely exhibit crystal-like structural order over nanoscale dimensions that are below the detection limits of X-ray diffraction measurements. Overall, the 2D intensity correlations indicate that sucrose adsorbs at calcium hydroxide sites, presumably inhibiting growth of $Ca(OH)_2$. These analyses unambiguously

DOI: 10.1021/jacs.5b00622
J. Am. Chem. Soc. 2015, 137, 8096−8112

establish that sucrose molecules adsorb structurally intact at nonhydrated silanol Q^0 and hydrated Q^1 and Q^2 silicate sites as well as on $Ca(OH)_2$ moieties and inhibit the reaction of surface silanol Q^0 species with water to effectively hinder hydration of silicate particle surfaces.

Proximities of Adsorbed Sucrose Molecules to Near-Surface Silicate Species. The partitioning of adsorbed sucrose molecules among nonhydrated and hydrated silicate species suggests that both the nucleation and growth of calcium silicate hydration products are inhibited. The different respective contributions from adsorption at different silicate sites can be assessed by probing the intermolecular interactions and relative proximities of adsorbed sucrose molecules to different silicate surface moieties by exploiting through-space dipole−dipole-couplings between their distinct NMR-active nuclei. Specifically, interactions between proximate ^{29}Si and ^{13}C nuclear spins in silicate and sucrose surface moieties, respectively, in tricalcium silicate hydrated with 0.1% bwos sucrose can be directly identified and quantified by using rotational-echo double-resonance (REDOR) NMR techniques[76] (in contrast to the DNP HETCOR measurements that correlate ^{29}Si to ^{13}C chemical shifts indirectly through ^{1}H chemical shifts). Such REDOR NMR methods are sensitive to the strengths of heteronuclear (^{29}Si−^{13}C) dipole−dipole couplings and rely on a series of radio frequency recoupling pulses to reintroduce heteronuclear dipolar spin couplings between nuclei of interest (e.g., ^{29}Si−^{13}C) that are otherwise averaged out under MAS conditions. The restoration of such dipolar spin couplings causes selective attenuation of NMR signals from dipole−dipole-coupled nuclei, the extent of which is determined by the strengths of the associated heteronuclear dipolar couplings. The REDOR technique, in combination with the dramatic signal sensitivity enhancement afforded by the surface-enhanced DNP NMR methods, enable the molecular proximities and interactions between dilute silicate moieties and adsorbed sucrose molecules at low-surface-area particle surfaces to be quantified. Solid-state 1D ^{29}Si{^{13}C} DNP REDOR measurements were recorded in two steps: one where the ^{29}Si and ^{13}C spins were not recoupled under conditions of MAS to yield a reference spectrum with ^{29}Si signal intensity (S_0) and a second where the ^{29}Si−^{13}C dipolar couplings were restored under MAS (by the application of dipolar recoupling π pulses on the ^{13}C channel) that yield a separate spectrum with attenuated ^{29}Si signal intensity (S). A subsequent ^{29}Si{^{13}C} REDOR difference spectrum exhibits signal intensity (ΔS) that is obtained by subtracting the signal intensities of the REDOR spectrum from the reference spectrum: $\Delta S = S_0 - S \geq 0$. The measured ^{29}Si signal intensity in the difference spectrum corresponds to near-surface ^{29}Si nuclei that are dipole−dipole-coupled to ^{13}C nuclei in the adsorbed sucrose molecules. For example, Figure 8a shows the ^{29}Si{^{13}C} DNP REDOR reference spectrum of tricalcium silicate hydrated (4 h, 90 °C) with 0.1% bwos ^{13}C-sucrose where the ^{29}Si−^{13}C spin pairs have been effectively decoupled under conditions of 10 kHz MAS. The spectrum with intensities S_0 exhibits overlapping ^{29}Si signals at −73, −79, and −85 ppm from silanol Q^0, hydrated Q^1 and Q^2 silicate species, respectively, present on the surfaces of hydrating tricalcium silicate particles as previously discussed. Similar ^{29}Si signals are observed in the ^{29}Si{^{13}C} DNP REDOR spectrum shown in Figure 8b, though with attenuated signal intensities (S) attributable to the reintroduction of ^{29}Si−^{13}C dipolar couplings. The extents of attenuated (dipolar-dephased) signal intensities between the two spectra (Figure 8a,b) are elucidated

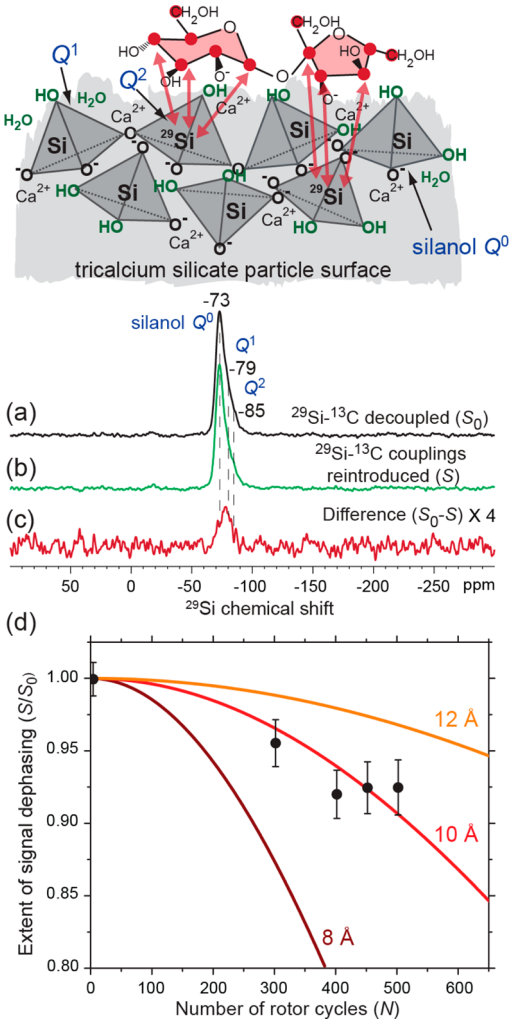

Figure 8. Solid-state surface-enhanced 1D ^{29}Si{^{13}C} DNP REDOR spectra of hydrated tricalcium silicate (4 h, 90 °C) with 0.1% bwos ^{13}C-labeled sucrose acquired (a) without or (b) with the application of recoupling pulses to reintroduce ^{29}Si−^{13}C heteronuclear dipole−dipole couplings. The spectra in a and b were acquired with 4 mM TEKPol (biradical) in frozen 1,2-dichlorobenzene (the DNP solvent), with continuous microwave irradiation at 263 GHz, at 9.4 T, 105 K, and 10 kHz MAS. The difference spectrum in c indicates the extent of attenuation of the ^{29}Si signal intensity from reintroduction of ^{29}Si−^{13}C dipolar interactions. (d) Extents of ^{29}Si signal attenuation plotted versus the number of MAS rotor cycles, as measured (black dots) in a series of 1D ^{29}Si{^{13}C} DNP REDOR S/S_0 (dipolar dephasing) experiments. The solid lines correspond to intensity decay curves determined theoretically for different mean interatomic ^{29}Si−^{13}C distances of 8, 10, and 12 Å. The inset in a shows a schematic diagram of silanol Q^0, Q^1 and Q^2 ^{29}Si surface nuclei in partially hydrated tricalcium silicate, along with the dipolar interactions (red arrows) with surface-adsorbed ^{13}C-sucrose nuclei (red circles) that cause dephasing of the DNP REDOR signal as manifested in c and d.

by the difference spectrum (ΔS) shown in Figure 8c, which yields distinct ^{29}Si signal intensity centered at −79 ppm over the range of −67 to −90 ppm. This ^{29}Si signal intensity in the difference spectrum corresponds exclusively to near-surface ^{29}Si nuclei that are dipolar-coupled to ^{13}C nuclei in the surface-adsorbed sucrose molecules.

The monolayer coverages of low-surface-area silicate particles by sucrose molecules result in distinct molecular-level site-specific interactions that indicate the different adsorption

DOI: 10.1021/jacs.5b00622
J. Am. Chem. Soc. 2015, 137, 8096−8112

selectivities of the sucrose molecules. Compared to the spectra in Figure 8a,b, the significantly reduced ^{29}Si signal intensity observed in the REDOR difference spectrum (signal-to-noise ratio = 4) in Figure 8c is consistent with the dilute quantities of interacting ^{29}Si−^{13}C nuclear spin pairs associated with surface species on low-surface-area silicate particles. Despite this low signal intensity, important differences can be identified by comparing the extent of ^{29}Si signal dephasing from chemically distinct ^{29}Si surface species observed in the REDOR difference spectrum (Figure 8c). For example, compared to the relative maximum in ^{29}Si signal intensity centered at −73 ppm in the reference (Figure 8a) and REDOR (Figure 8b) spectra, the REDOR difference spectrum (Figure 8c) exhibits a relative maximum in ^{29}Si signal intensity that is clearly displaced (by 6 ppm) to ca. −79 ppm, the region that is associated with the hydrated Q^1 and Q^2 silicate species. Consequently, the extents of ^{29}Si signal dephasing in the REDOR measurements are greater for the hydrated Q^1 and Q^2 silicate species. Therefore, the ^{13}C nuclei from adsorbed sucrose molecules are shown to be in closer molecular-level proximities to ^{29}Si nuclei in Q^1 and Q^2 species (i.e., in calcium silicate hydrates) present at particle surfaces.[101] This suggests that sucrose molecules adsorbed strongly at calcium silicate hydrates effectively slow subsequent growth, which is consistent with results from previous calorimetry and neutron scattering measurements of silicate−water mixtures hydrated in the presence of sucrose.[83,102] The analyses of the DNP REDOR measurements thus establish that sucrose molecules are molecularly near silanol Q^0 and hydrated Q^1 and Q^2 silicate surface species, with evidence for stronger or preferential adsorption at the hydrated silicate sites, which until now have not been elucidated because of the dilute concentrations of hydrated species and low signal sensitivity of conventional NMR techniques.[28]

The proximities of NMR-active nuclei in adsorbed sucrose molecules to near-surface silicate species can be estimated on the basis of the strengths of their distance-dependent dipole−dipole interactions. Specifically, REDOR experiments can be used to quantify mean internuclear distances between such dipole−dipole-coupled ^{13}C and ^{29}Si spin pairs. The associated heteronuclear dipolar couplings between the spin pairs are averaged under MAS conditions to enhance spectral resolution. Such dipolar couplings can nevertheless be reintroduced under MAS conditions by applying a series of recoupling π pulses, with the extent of recoupling depending on the number of MAS rotor cycles (N). For example, the normalized signal intensity (S/S_0) determined from a series of 1D ^{29}Si{^{13}C} DNP REDOR experiments are plotted as a function of the number of MAS rotor cycles (N) (black solid circles), the latter of which is proportional to the total recoupling time (Figure 8d). Intensities S/S_0 are observed to become smaller with increasing values of N, which reflect dipole−dipole interactions between ^{13}C nuclei in adsorbed sucrose molecules and near-surface ^{29}Si nuclei. The normalized signal intensity (S/S_0) decay can be theoretically modeled for different internuclear distances in a system of dipole−dipole-coupled spin pairs[103] and subsequently compared to the experimentally measured S/S_0 values.

For ^{13}C-labeled sucrose used here, the ^{29}Si{^{13}C} DNP REDOR analysis is complicated by multispin dipole−dipole interactions as well as by contributions from a distribution of ^{29}Si−^{13}C internuclear distances, notably from subsurface silicate species and different configurations of adsorbed sucrose molecules. In the case of isolated dipole−dipole-coupled spin pairs, which would be the case for isotopically dilute NMR-active nuclei (e.g., natural abundance ^{13}C and ^{29}Si), a two-spin system can be used to model the decay of intensities S/S_0. However, this is not the case for systems for NMR-active nuclei with high natural abundances, strong dipole interactions, or high levels of isotopic enrichment, the latter being the case for the ^{13}C-labeled sucrose used here. However, without isotopic ^{13}C enrichment of the adsorbed sucrose molecules, low NMR signal sensitivity renders the ^{29}Si{^{13}C} REDOR measurements infeasible, even with DNP signal enhancement. The use of ^{13}C-labeled sucrose is therefore necessary to achieve feasible signal sensitivity, and the resulting ^{29}Si{^{13}C} DNP REDOR measurements and analysis yield semiquantitative estimates for the proximities between the adsorbed sucrose molecules and silicate species near heterogeneous particle surfaces.

Recognizing the unavoidable challenges arising from the use of ^{13}C-labeled sucrose, a two-spin model can nevertheless be used to approximate the mean distances between dipole−dipole-coupled ^{13}C and ^{29}Si nuclei associated with near-surface species. The theoretical intensity buildup curves from such an analysis (details in Supporting Information) are shown as solid lines in Figure 8d for mean ^{29}Si−^{13}C internuclear distances of 8 Å (brown), 10 Å (red), and 12 Å (orange), which exhibit different extents of S/S_0 intensity attenuation for increasing values of N. Comparison of these theoretical buildup curves with the experimental normalized intensities (black solid circles) indicates that the mean ^{29}Si−^{13}C interatomic distance between ^{29}Si silicate nuclei and the ^{13}C nuclei in surface-adsorbed sucrose is approximately 10 Å. Analogously, the experimental signal buildup curve was also compared with theoretical buildup curves for Gaussian distributions of ^{29}Si−^{13}C interatomic distances (Supporting Information), which yield similar estimates (10−11 Å). It should be noted that these estimates represent average internuclear ^{29}Si−^{13}C distances between ^{13}C nuclei in adsorbed sucrose and ^{29}Si nuclei associated with silanol and hydrated silicate species near the particle surfaces. In particular, subsurface ^{29}Si nuclei are also expected to contribute to the distance analysis because of efficient ^{1}H−^{1}H spin diffusion within the hydrated surface layers and the high sensitivity of the DNP-enhanced REDOR measurements. Compared to ^{13}C nuclei in sucrose molecules that are adsorbed on and dipole−dipole-coupled to the outermost ^{29}Si surface species, subsurface ^{29}Si nuclei are more distant from and therefore less strongly coupled to the ^{13}C nuclei. The broad correlated intensity distributions in the 2D ^{13}C{^{1}H} DNP HETCOR spectrum discussed above corroborate such a distribution of ^{29}Si−^{13}C internuclear distances, which reflects contributions from more distant subsurface ^{29}Si nuclei and diverse molecular configurations of adsorbed sucrose. Such contributions are expected to skew the mean internuclear distance to larger values, consistent with the 10 Å estimated by the DNP REDOR analysis.

In summary, for tricalcium silicate hydrated with sucrose, the 2D DNP HETCOR analyses establish strong intermolecular interactions between sucrose molecules and −SiOH and −CaOH moieties associated with dilute, but nevertheless distinct, silicate hydration products present at particle surfaces. These molecular-level interactions account for the strong adsorption of sucrose molecules near or at $Ca(OH)_2$, silanol Q^0, and calcium silicate hydrate species (e.g., hydrated Q^1 and Q^2). Such adsorption is likely mediated by hydrogen bonds between the carbinol moieties on the sucrose molecules and −SiOH groups as well as by electrostatic interactions of

DOI: 10.1021/jacs.5b00622
J. Am. Chem. Soc. 2015, 137, 8096−8112

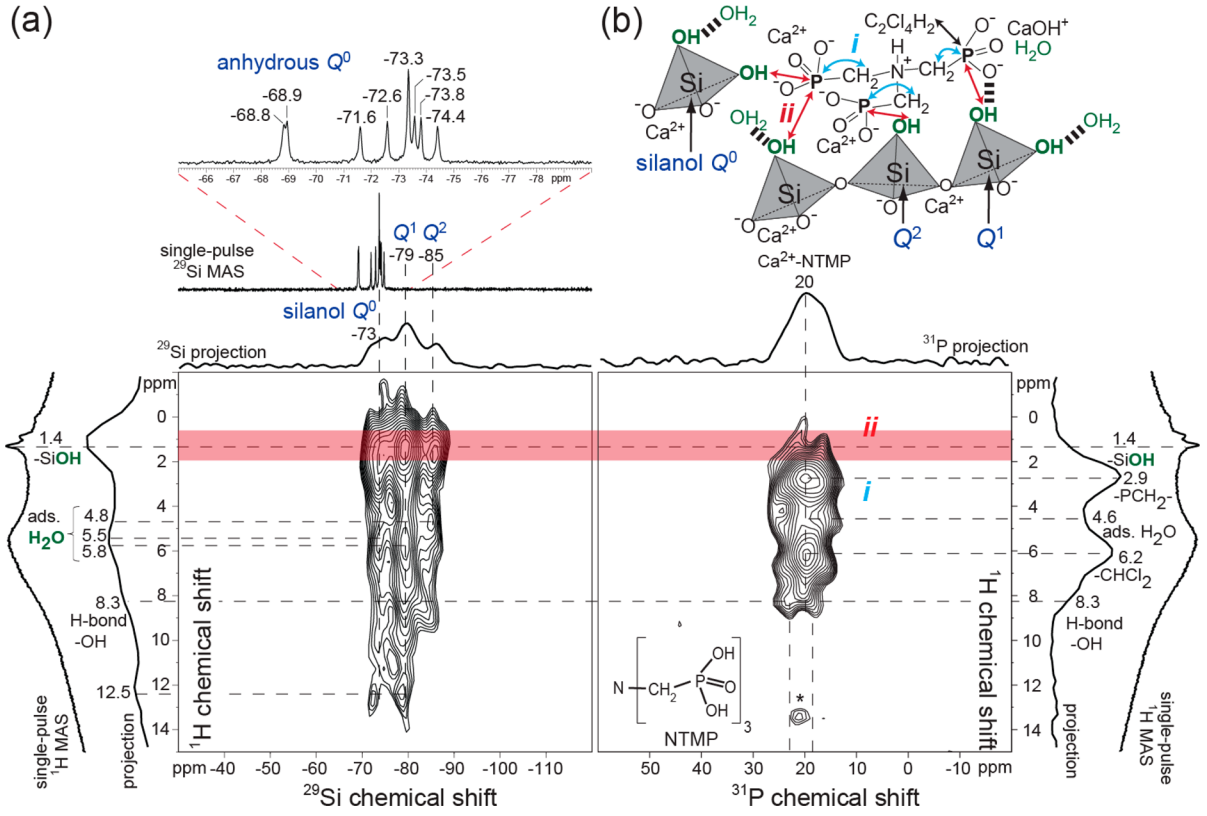

Figure 9. Solid-state 2D (a) ^{29}Si{^{1}H} and (b) ^{31}P{^{1}H} DNP HETCOR spectra of hydrated tricalcium silicate (4 h, 90 °C) with 0.1% bwos of NTMP (pH 12.7) acquired with (a) 4 mM TEKPol in frozen 1,2-dichlorobenzene (the DNP solvent) or (b) 2 mM bCTbK in frozen 1,1,2,2-tetrachloroethane (the DNP solvent), with continuous microwave irradiation at 263 GHz, at 9.4 T, 105 K, and (a) 8 kHz or (b) 12.5 kHz MAS. The experimentally measured ^{29}Si and ^{31}P DNP NMR surface signal enhancements (ε_{Si} and ε_P, respectively) were approximately 10 and 5, respectively. The 2D spectra were recorded over total experimental times of (a) 7 h and (b) 1 h. Solid-state 1D single-pulse ^{29}Si and ^{1}H MAS spectra acquired at 11.7 T, 25 °C, and 10 kHz MAS are shown along the (a) horizontal and (a and b) vertical axes for comparison with the 1D projections of the 2D spectra. The inset (b, top) shows a schematic diagram of silanol Q^0 and partially cross-linked Q^1 and Q^2 ^{29}Si species in tricalcium silicate hydration products, along with their (*i*) intramolecular (blue arrows) and (*ii*) intermolecular (red arrows) dipolar interactions with −SiOH species, methylene groups, coadsorbed water, and 1,1,2,2-tetrachloroethane (DNP solvent) as established by the intensity correlations in the 2D spectra. The inset (b, bottom left) shows a schematic structure of a fully protonated NTMP molecule. * in b indicates correlated intensity in the 2D spectrum that is an artifact, which arises from the experimental ^{1}H carrier frequency. The isotropic chemical shifts of ^{1}H (vertical axes) and (a) ^{29}Si or (b) ^{31}P species (horizontal axes) are labeled above or alongside their respective NMR signals.

partially deprotonated carbinol sucrose moieties with Ca^{2+} cations at the particle surfaces. Moreover, the DNP REDOR results establish the propensity of sucrose molecules to adsorb preferentially at the hydrated (Q^1 and Q^2) silicate sites, compared to silanol Q^0 sites. Such competitive adsorption of sucrose molecules in place of water at silanol Q^0 and hydrated silicate sites slow the rates of surface hydration processes, which have important implications for the rheological and mechanical properties of tricalcium silicate−water mixtures.

Phosphonate-Mediated Hydration of Tricalcium Silicate. Dilute quantities (0.1% bwos) of phosphonic acid molecules, like sucrose, strongly inhibit silicate hydration processes at low-surface-area particles. Such low absolute quantities of phosphonic acid species also correspond to approximately monolayer coverages of the silicate particles (analysis in Supporting Information). Notably, although both organic molecules exhibit similar macroscopic effects on hydration, they have markedly different molecular architectures that are expected to manifest distinct adsorption interactions at silicate particle surfaces. Whereas the hydroxyl groups of sucrose (pK_a 12.6) interact principally via hydrogen bonding to silanol or hydrated silicate surface moieties, hydroxyl groups on NTMP molecules ($N[CH_2PO(OH)_2]_3$, Chart 1) deprotonate under highly alkaline solution conditions (pH >12), leading to principally electrostatic interactions with the silicate surface. NTMP molecules possess three equivalent four-coordinated phosphorus atoms that are each covalently bonded to two hydroxyl groups. The six ionizable proton moieties dissociate sequentially under different pH conditions (with pK_a values of 1.4, 4.6, 5.9, 7.2, and 12.8 for the dissociation of the second through the sixth protons, respectively)[104,105] to yield NTMP anions that are increasingly negatively charged. As a consequence, under the alkaline solution conditions used here (pH 12.7), anionic $NTMP^{6-}$ and $NTMP^{5-}$ species are expected to be principally present and interact electrostatically with Ca^{2+} cations to form calcium phosphonate (Ca^{2+}-NTMP) complexes at or near the silicate particle surfaces. Previous studies of the chelating properties of phosphonic acids, including NTMP, for mono-, di-, and trivalent cations have established the chemical kinetics of cation−phosphonate complexation.[106,107] NTMP molecules thus principally interact electrostatically at tricalcium silicate particle surfaces, competing with water, to inhibit surface hydration effectively.

As for sucrose, the influences of dilute quantities of NTMP on hydration of low-surface-area silicate particles can be established by using solid-state NMR measurements to

DOI: 10.1021/jacs.5b00622
J. Am. Chem. Soc. 2015, 137, 8096−8112

understand their different adsorption properties. Specifically, the ^{29}Si MAS NMR spectrum of tricalcium silicate hydrated with 0.1% bwos NTMP (Figure 9a, top) reveals eight ^{29}Si signals from −68 to −75 ppm from chemically distinct anhydrous Q^0 ^{29}Si sites from bulk particle anhydrous silicate species, similar to those observed for tricalcium silicate hydrated in the presence of sucrose (Figure 6a). By comparison, with NTMP no detectable ^{29}Si signals are observed at −79 and −85 ppm from hydrated Q^1 and Q^2 silicate moieties, respectively, within the sensitivity limits of the conventional NMR measurement. This establishes that no detectable quantities of calcium silicate hydrates are formed under these conditions (4 h, 90 °C), as observed for similar sucrose compositions (0.1% bwos). (Previous molecular-level studies in the literature used loadings of NTMP that were an order of magnitude higher (1−3% bwos) to control hydration.)[24] The results presented here establish that, despite the different molecular architectures of sucrose and NTMP, dilute concentrations of both organic molecules strongly inhibit silicate hydration.

The influences of NTMP molecules on tricalcium silicate hydration are expected to be due to their strong electrostatic adsorption interactions at the particle surfaces. Such molecular interactions are established by solid-state surface-enhanced 2D ^{29}Si{^{1}H} and ^{31}P{^{1}H} DNP HETCOR measurements, which provide direct evidence for interactions between adsorbed Ca^{2+}-NTMP species and surface silicate moieties. For example, the solid-state 2D ^{29}Si{^{1}H} DNP HETCOR spectrum of tricalcium silicate hydrated (4 h, 90 °C) in the presence of 0.1% bwos NTMP shown in Figure 9a exhibits strong correlated intensity between different ^{1}H and ^{29}Si signals associated with distinct silicate hydration products. Specifically, the DNP-enhanced ^{29}Si signals at −73 ppm (from silanol Q^0), −79 ppm (from Q^1), and −85 ppm (from Q^2) are correlated with the ^{1}H signal at 1.4 ppm from silanol groups (−SiOH), which unambiguously establish the presence of surface hydration products, even in the presence of NTMP. Intermolecular intensity correlations are observed between signals at −73, −79, and −85 ppm in the ^{29}Si dimension and the ^{1}H signals at 5.5, 5.8, and 4.8 ppm, respectively, from coadsorbed water present near silanol Q^0, and Q^1 and Q^2 ^{29}Si species at the particle surfaces. The spectrum reveals additional intensity correlations between ^{29}Si signals at −73 and −79 ppm and ^{1}H signals at 8.3 and 12.5 ppm that arise from hydrogen-bonded hydroxyl groups.[11] In addition, although the signal intensities in the 2D ^{29}Si{^{1}H} DNP HETCOR spectrum are not strictly quantitative, their comparison for different ^{29}Si silicate moieties reflects the presence of a greater fraction of hydrated Q^1 and Q^2 silicate species at particle surfaces in the presence of 0.1% bwos NTMP than that for tricalcium silicate hydrated with 0.1% bwos sucrose (Figure 6c). This is in direct opposition to the conclusion that would be drawn by comparison with conventional NMR results, highlighting the importance of the new insights that are enabled by surface-enhanced DNP NMR methods. Such increased surface fractions of Q^1 and Q^2 species are consistent with the enhanced initial dissolution of Ca^{2+} cations from tricalcium silicate particle surfaces that is promoted by the acidic NTMP species.[24,108] Such rapid dissolution of inorganic species (e.g., Ca^{2+}, $Si(OH)_3O^-$, and $Si(OH)_4$) is followed by their reaction with water, resulting in the formation of very small (<2 wt %) quantities of calcium silicate hydrates that are nevertheless manifested in the 2D ^{29}Si{^{1}H} DNP HETCOR spectrum. The analyses provide detailed insights regarding the distributions and mutual molecular interactions of hydroxyl moieties, water molecules, and silicate species present at particle surfaces with approximately monolayer coverages of adsorbed NTMP molecules.

The intermolecular interactions that account for the adsorption behaviors of NTMP molecules at particle surfaces are correlated to their molecular structures and reaction properties. Direct evidence of specific intermolecular interactions between dilute adsorbed NTMP (0.1% bwos) and tricalcium silicate species is provided by complementary 2D ^{31}P{^{1}H} DNP HETCOR analyses. For such measurements, the high natural abundance (100%) of ^{31}P eliminates the need for expensive isotopic enrichment, even for dilute quantities of NTMP adsorbed on silicate particles. As shown in Figure 9b, a 2D ^{31}P{^{1}H} DNP HETCOR spectrum provides improved signal sensitivity and ^{1}H resolution, compared to the accompanying ^{1}H MAS spectrum (Figure 9b, right), and reveals correlated intensities between distinct ^{31}P and ^{1}H signals from surface species. Specifically, strong correlated intensity is observed between the ^{31}P signal at 20 ppm and the ^{1}H signal at 2.9 ppm, which arises from intramolecular interactions associated with the $-PCH_2-$ moieties in Ca^{2+}-NTMP complexes (labeled *i* in the schematic diagram of Figure 9b). This ^{31}P signal assignment is based on separate solid-state ^{31}P NMR measurements of neat Ca^{2+}-NTMP (Supporting Information, Figure S7). The 2D spectrum also reveals strong correlated intensity at 20 ppm in the ^{31}P dimension and at 6.2 ppm in the ^{1}H dimension (from $-CHCl_2$ moieties), which reflects interactions between the Ca^{2+}-NTMP species and 1,1,2,2-tetrachloroethane DNP-solvent molecules. Most importantly, intermolecular interactions account for the correlated intensity observed between the ^{31}P signal at 20 ppm and the ^{1}H signal at 1.4 ppm, the latter from silanol groups (−SiOH) previously assigned above (on the basis of the 2D ^{29}Si{^{1}H} DNP HETCOR spectrum in Figure 9a). This establishes that the Ca^{2+}-NTMP species are in close (<1 nm) molecular proximity to −SiOH moieties associated with surface silanol Q^0 (nonhydrated) and hydrated silicate (Q^1 and Q^2) species. By comparison, correlated intensity is not resolved in the 2D ^{29}Si{^{1}H} DNP HETCOR spectrum (Figure 9a) between different ^{29}Si signals and the ^{1}H signal at 2.9 ppm from $-PCH_2-$ moieties, consistent with relatively weak dipole−dipole couplings between these more distant moieties. The NTMP molecules are expected to bind to surface sites through electrostatic interactions with Ca^{2+} cations, as depicted in the schematic diagram of Figure 9b. The correlated ^{1}H signal intensity at 1.4 ppm is weaker than that associated with intramolecular interactions (see above), consistent with weaker intermolecular dipole−dipole couplings. In addition, correlated 2D intensity is observed between the ^{31}P signal centered at 20 ppm and the ^{1}H signal at 8.3 ppm associated with hydrogen-bonded −SiOH groups. This intensity correlation manifests two partially resolved ^{31}P signals that are attributed to different extents of protonation of the NTMP molecules (e.g., $NTMP^{5-}$ vs $NTMP^{6-}$)[104,107] that yield different local ^{31}P environments in the Ca^{2+}-NTMP species. Under the strongly alkaline solution conditions used here (pH 12.7), at most one of the six ionizable proton moieties is expected to be associated with a given NTMP molecule (pK_{a1} 12.8). Consequently, the NTMP molecules are expected to be highly negatively charged and thus adsorb at cationic silicate surfaces principally via

DOI: 10.1021/jacs.5b00622
J. Am. Chem. Soc. 2015, 137, 8096−8112

electrostatic interactions, with minor contributions from hydrogen bonding to nearby −SiOH moieties. Notably, unlike sucrose, the relative extents of electrostatic and hydrogen-bonding interactions of NTMP molecules can be facilely adjusted by controlling solution pH. Such nuanced differences in the compositions and structures of low-surface-area solids are thus detected and resolved by the 2D DNP HETCOR measurements. The resulting analyses unambiguously establish the presence of silanol and hydrated silicate moieties near tricalcium silicate particle surfaces, even in the presence of dilute surface-adsorbed NTMP, along with their mutual interactions that inhibit further hydration.

Consequently, although dilute concentrations of NTMP or sucrose molecules both hinder silicate hydration to similar extents, they do so via significantly different adsorption behaviors that arise from their distinct molecular architectures and corresponding interactions under alkaline solution conditions. In contrast to NTMP, sucrose molecules predominantly adsorb through hydrogen bonding between their carbinol moieties and the −SiOH groups on silanol Q^0, portlandite, or calcium silicate hydrate sites, with evidence for stronger or preferential adsorption on calcium silicate hydrates. The DNP NMR results support the different adsorption characteristics exhibited by low absolute concentrations of sucrose and NTMP molecules at tricalcium silicate particle surfaces and provide new insights regarding the organic-mediated hydration chemistry of silicate−water mixtures. Macroscopic hydration is effectively inhibited by approximately monolayer coverages of silicate particles by organic molecules, which competitively adsorb in place of water. Importantly, under these industrially relevant compositions, there are no excess multilayers of adsorbed molecules that otherwise represent an additional diffusion barrier to water, which is present at higher concentrations of organic species. Adsorption of dilute organic species at silanol Q^0 (nonhydrated) surface sites restricts the adsorption of water, consequently hindering hydration reactions that would otherwise proceed because of the dissolution of ions (e.g., $H_3SiO_4^-$ and Ca^{2+}) and partial polymerization of the silanol Q^0 species to yield calcium silicate hydrates (Q^1 and Q^2 species). The organic molecules can also adsorb directly on early stage silicate hydration products, including calcium silicate hydrates and portlandite ($Ca(OH)_2$), to slow or limit their further growth.[14] The results presented here therefore establish that formation of silicate hydration products is inhibited by the competitive adsorption of dilute organic species versus water on low-surface-area particles. The different molecular architectures and interactions of such dilute organic species correlate with their different adsorption behaviors, which yield surprisingly similar influences on the rates of surface hydration phenomena.

CONCLUSIONS

The effects of sucrose and phosphonic acid molecules on surface hydration of tricalcium silicate particles, although macroscopically similar, are shown to result from very different adsorption behaviors associated with their distinct molecular architectures. Until now, such subtle differences in the competitive adsorption of dilute organic molecules in place of water at silicate surfaces have been exceedingly challenging and often infeasible to establish because of low absolute concentrations of organic species, low particle surface areas, low isotopic natural abundances of NMR-active species, and low sensitivities of conventional NMR techniques. By comparison, recently introduced surface-enhanced DNP NMR methods provide significantly improved sensitivity that enable dilute surface-adsorbed species to be measured and analyzed in industrially important systems. These include solid-state 2D $^{13}C\{^1H\}$, $^{29}Si\{^1H\}$, $^{31}P\{^1H\}$ DNP HETCOR, and $^{29}Si\{^{13}C\}$ DNP REDOR measurements of dilute (∼0.1% bwos) sucrose or phosphonic acid species that are used to mediate hydration of low-surface-area (∼1 m^2/g, nonporous) tricalcium silicate, an industrially important cementitious material.

The analyses yield insights on the molecular interactions that underlie organic-mediated hydration at silicate surfaces, which directly affect the rheological and mechanical properties of cement−water mixtures. Specifically, the DNP NMR results establish that sucrose molecules adsorb at silanol and silicate hydration products, notably calcium silicate hydrates and calcium hydroxide (portlandite), principally via hydrogen-bonding interactions. Furthermore, the measurements provide evidence for stronger or preferential adsorption of sucrose at the hydrated silicate sites compared to that at the silanol sites. Additionally, the results also suggest that partially deprotonated carbinol groups likely interact electrostatically with Ca^{2+} cations that are expected to facilitate surface adsorption of sucrose. Such adsorption behaviors are correlated with the specific stereochemistry of the disaccharide molecules and their stability under alkaline conditions because of the nonreducing character of the $\alpha-\beta$ glycosidic bonding configuration. By comparison, under alkaline conditions NTMP molecules adsorb strongly but nonselectively at or near silanol and hydrated silicate species principally via electrostatic interactions to form Ca^{2+}-NTMP complexes at particle surfaces. In general, phosphonic or related organic acids with multiple ionizable proton moieties present opportunities to adjust the relative extents by which the acids interact electrostatically or through hydrogen bonds with inorganic oxide surfaces. Thus, although sucrose and NTMP inhibit hydration of surface silicate species by competing with water for adsorption sites, their respective surface interactions are notably different because of their distinct molecular architectures. The analyses and insights presented here are expected to provide criteria for the rational design and use of adsorbate species to mediate reaction processes at heterogeneous inorganic oxide surfaces, including hydration, dissolution, crystallization, corrosion or adhesion.

ASSOCIATED CONTENT

Supporting Information

Additional solid-state 1D and 2D NMR spectra, experimentally measured ^1H and ^{13}C DNP NMR signal enhancements, and details of experimental and simulated DNP REDOR spectra. The Supporting Information is available free of charge on the ACS Publications website at DOI: 10.1021/jacs.5b00622.

AUTHOR INFORMATION

Corresponding Author

*bradc@engineering.ucsb.edu

Notes

The authors declare no competing financial interest.

ACKNOWLEDGMENTS

This work was supported in part by Halliburton, Inc., and by the U.S. Federal Highway Administration (FHWA) under agreement no. DTFH61-12-H-00003. We thank Dr. M. Caporini and Dr. M. Rosay for helpful discussions concerning

DOI: 10.1021/jacs.5b00622
J. Am. Chem. Soc. 2015, 137, 8096−8112

the DNP NMR measurements, and Bruker Biospin Corp., Billerica, Massachusetts, USA, for access to the DNP NMR instrumentation. We are grateful to Prof. H. Oschkinat and Dr. W. T. Franks for access to the DNP NMR facilities at the Leibniz-Institute für Molekulare Pharmakologie (FMP), Berlin, Germany, where initial measurements were conducted. We also thank Prof. P. Tordo and Dr. O. Ouari (Aix-Marseille Université, France) for providing the biradicals used in the DNP NMR experiments. Characterization measurements were conducted using the Central Facilities of the UCSB Materials Research Laboratory (MRL) that are supported by the MRSEC program of the U.S. National Science Foundation under award no. DMR-1121053. The MRL Central Facilities are a member of the NSF-funded Materials Research Facilities Network (www.mrfn.org). DNP NMR measurements were conducted at the Centre de RMN à Très Hauts Champs at the École Normale Supérieure, Lyon, France, with technical support from Lénaic Leroux. Financial support for the DNP NMR studies is acknowledged from EQUIPEX contract ANR-10-EQPX-47-01 and ERC Advanced grant no. 320860. B.F.C. was a Professeur Invité at the ENS-Lyon during portions of 2012 and 2013.

REFERENCES

(1) Salvalaglio, M.; Vetter, T.; Giberti, F.; Mazzotti, M.; Parrinello, M. *J. Am. Chem. Soc.* **2012**, *134*, 17221−17233.
(2) Kuvadia, Z. B.; Doherty, M. F. *Cryst. Growth Des.* **2013**, *13*, 1412−1428.
(3) Rimer, J. D.; An, Z.; Zhu, Z.; Lee, M. H.; Goldfarb, D. S.; Wesson, J. A.; Ward, M. D. *Science* **2010**, *330*, 337−341.
(4) Berman, A.; Addadi, L.; Weiner, S. *Nature* **1988**, *331*, 546−548.
(5) De Yoreo, J. J.; Dove, P. M. *Science* **2004**, *306*, 1301−1302.
(6) Wise, E. R.; Maltsev, S.; Davies, M. E.; Duer, M. J.; Jaeger, C.; Loveridge, N.; Murray, R. C.; Reid, D. G. *Chem. Mater.* **2007**, *19*, 5055−5057.
(7) Akiva-Tal, A.; Kababya, S.; Balazs, Y. S.; Glazer, L.; Berman, A.; Sagi, A.; Schmidt, A. *Proc. Natl. Acad. Sci. U.S.A.* **2011**, *108*, 14763−14768.
(8) Wang, Y.; Von Euw, S.; Fernandes, F. M.; Cassaignon, S.; Selmane, M.; Laurent, G.; Pehau-Arnaudet, G.; Coelho, C.; Bonhomme-Coury, L.; Giraud-Guille, M.-M.; Babonneau, F.; Azaïs, T.; Nassif, N. *Nat. Mater.* **2013**, *12*, 1144−1153.
(9) Zeng, H.; Hwang, D. S.; Israelachvili, J. N.; Waite, J. H. *Proc. Natl. Acad. Sci. U.S.A.* **2010**, *107*, 12850−12853.
(10) Taylor, H. F. W. *Cement Chemistry*; Academic Press: London, 1990.
(11) Rawal, A.; Smith, B. J.; Athens, G. L.; Edwards, C. L.; Roberts, L.; Gupta, V.; Chmelka, B. F. *J. Am. Chem. Soc.* **2010**, *132*, 7321−7337.
(12) Zhang, L.; Catalan, L. J. J.; Balec, R. J.; Larsen, A. C.; Esmaeili, H. H.; Kinrade, S. D. *J. Am. Ceram. Soc.* **2010**, *93*, 279−287.
(13) Smith, B. J.; Rawal, A.; Funkhouser, G. P.; Roberts, L. R.; Gupta, V.; Israelachvili, J. N.; Chmelka, B. F. *Proc. Natl. Acad. Sci. U.S.A.* **2011**, *108*, 8949−8954.
(14) Cheung, J.; Jeknavorian, A.; Roberts, L.; Silva, D. *Cem. Concr. Res.* **2011**, *41*, 1289−1309.
(15) Skibsted, J.; Hall, C. *Cem. Concr. Res.* **2008**, *38*, 205−225.
(16) Skibsted, J.; Jakobsen, H. J.; Hall, C. *J. Chem. Soc., Faraday Trans.* **1995**, *91*, 4423−4430.
(17) Le Saout, G.; Lécolier, E.; Rivereau, A.; Zanni, H. *Cem. Concr. Res.* **2006**, *36*, 71−78.
(18) Andersen, M. D.; Jakobsen, H. J.; Skibsted, J. *Cem. Concr. Res.* **2006**, *36*, 3−17.
(19) Poulsen, S. L.; Kocaba, V.; Le Saoût, G.; Jakobsen, H. J.; Scrivener, K. L.; Skibsted, J. *Solid State Nucl. Magn. Reson.* **2009**, *36*, 32−44.
(20) Thomas, J. J.; Allen, A. J.; Jennings, H. M. *J. Phys. Chem. C* **2009**, *113*, 19836−19844.
(21) MacDonald, J. L.; Werner-Zwanziger, U.; Chen, B.; Zwanziger, J. W.; Forgeron, D. *Solid State Nucl. Magn. Reson.* **2011**, *40*, 78−83.
(22) Sevelsted, T. F.; Herfort, D.; Skibsted, J. *Cem. Concr. Res.* **2013**, *52*, 100−111.
(23) Bruere, G. M. *Nature* **1966**, *212*, 502−503.
(24) Bishop, M.; Bott, S. G.; Barron, A. R. *Chem. Mater.* **2003**, *15*, 3074−3088.
(25) Ridi, F.; Fratini, E.; Mannelli, F.; Baglioni, P. *J. Phys. Chem. B* **2005**, *109*, 14727−14734.
(26) Bishop, M.; Barron, A. R. *Ind. Eng. Chem. Res.* **2006**, *45*, 7042−7049.
(27) Poinot, T.; Govin, A.; Grosseau, P. *Cem. Concr. Res.* **2013**, *44*, 69−76.
(28) Smith, B. J.; Roberts, L. R.; Funkhouser, G. P.; Gupta, V.; Chmelka, B. F. *Langmuir* **2012**, *28*, 14202−14217.
(29) Rottstegge, J.; Wilhelm, M.; Spiess, H. W. *Cem. Concr. Compos.* **2006**, *28*, 417−426.
(30) Pawsey, S.; McCormick, M.; De Paul, S.; Graf, R.; Lee, Y. S.; Reven, L.; Spiess, H. W. *J. Am. Chem. Soc.* **2003**, *125*, 4174−4184.
(31) Maly, T.; Debelouchina, G. T.; Bajaj, V. S.; Hu, K.-N.; Joo, C.-G.; Mak-Jurkauskas, M. L.; Sirigiri, J. R.; van der Wel, P. C. A.; Herzfeld, J.; Temkin, R. J.; Griffin, R. G. *J. Chem. Phys.* **2008**, *128*, 052211.
(32) Lesage, A.; Lelli, M.; Gajan, D.; Caporini, M. A.; Vitzthum, V.; Miéville, P.; Alauzun, J.; Roussey, A.; Thieuleux, C.; Mehdi, A.; Bodenhausen, G.; Copéret, C.; Emsley, L. *J. Am. Chem. Soc.* **2010**, *132*, 15459−15461.
(33) Ni, Q. Z.; Daviso, E.; Can, T. V.; Markhasin, E.; Jawla, S. K.; Swager, T. M.; Temkin, R. J.; Herzfeld, J.; Griffin, R. G. *Acc. Chem. Res.* **2013**, *46*, 1933−1941.
(34) Rossini, A. J.; Zagdoun, A.; Lelli, M.; Lesage, A.; Copéret, C.; Emsley, L. *Acc. Chem. Res.* **2013**, *46*, 1942−1951.
(35) Hall, D. A.; Maus, D. C.; Gerfen, G. J.; Inati, S. J.; Becerra, L. R.; Dahlquist, F. W.; Griffin, R. G. *Science* **1997**, *276*, 930−932.
(36) Mak-Jurkauskas, M. L.; Bajaj, V. S.; Hornstein, M. K.; Belenky, M.; Griffin, R. G.; Herzfeld, J. *Proc. Natl. Acad. Sci. U.S.A.* **2008**, *105*, 883−888.
(37) Bayro, M. J.; Debelouchina, G. T.; Eddy, M. T.; Birkett, N. R.; MacPhee, C. E.; Rosay, M.; Maas, W. E.; Dobson, C. M.; Griffin, R. G. *J. Am. Chem. Soc.* **2011**, *133*, 13967−13974.
(38) Reggie, L.; Lopez, J. J.; Collinson, I.; Glaubitz, C.; Lorch, M. *J. Am. Chem. Soc.* **2011**, *133*, 19084−19086.
(39) Linden, A. H.; Lange, S.; Franks, W. T.; Akbey, Ü.; Specker, E.; van Rossum, B.-J.; Oschkinat, H. *J. Am. Chem. Soc.* **2011**, *133*, 19266−19269.
(40) Sergeyev, I. V.; Day, L. A.; Goldbourt, A.; McDermott, A. E. *J. Am. Chem. Soc.* **2011**, *133*, 20208−20217.
(41) Potapov, A.; Yau, W.-M.; Tycko, R. *J. Magn. Reson.* **2013**, *231*, 5−14.
(42) Wang, T.; Park, Y. B.; Caporini, M. A.; Rosay, M.; Zhong, L.; Cosgrove, D. J.; Hong, M. *Proc. Natl. Acad. Sci. U.S.A.* **2013**, *110*, 16444−16449.
(43) Takahashi, H.; Ayala, I.; Bardet, M.; De Paëpe, G.; Simorre, J.-P.; Hediger, S. *J. Am. Chem. Soc.* **2013**, *135*, 5105−5110.
(44) Debelouchina, G. T.; Bayro, M. J.; Fitzpatrick, A. W.; Ladizhansky, V.; Colvin, M. T.; Caporini, M. A.; Jaroniec, C. P.; Bajaj, V. S.; Rosay, M.; MacPhee, C. E.; Vendruscolo, M.; Maas, W. E.; Dobson, C. M.; Griffin, R. G. *J. Am. Chem. Soc.* **2013**, *135*, 19237−19247.
(45) Lelli, M.; Gajan, D.; Lesage, A.; Caporini, M. A.; Vitzthum, V.; Miéville, P.; Héroguel, F.; Rascón, F.; Roussey, A.; Thieuleux, C.; Boualleg, M.; Veyre, L.; Bodenhausen, G.; Copéret, C.; Emsley, L. *J. Am. Chem. Soc.* **2011**, *133*, 2104−2107.
(46) Lafon, O.; Rosay, M.; Aussenac, F.; Lu, X.; Trébosc, J.; Cristini, O.; Kinowski, C.; Touati, N.; Vezin, H.; Amoureux, J.-P. *Angew. Chem., Int. Ed.* **2011**, *50*, 8367−8370.
(47) Rossini, A. J.; Zagdoun, A.; Lelli, M.; Gajan, D.; Rascón, F.; Rosay, M.; Maas, W. E.; Copéret, C.; Lesage, A.; Emsley, L. *Chem. Sci.* **2012**, *3*, 108−115.

DOI: 10.1021/jacs.5b00622
J. Am. Chem. Soc. 2015, 137, 8096−8112

(48) Lee, D.; Takahashi, H.; Thankamony, A. S. L.; Dacquin, J.-P.; Bardet, M.; Lafon, O.; De Paëpe, G. *J. Am. Chem. Soc.* **2012**, *134*, 18491−18494.
(49) Rossini, A. J.; Zagdoun, A.; Lelli, M.; Canivet, J.; Aguado, S.; Ouari, O.; Tordo, P.; Rosay, M.; Maas, W. E.; Copéret, C.; Farrusseng, D.; Emsley, L.; Lesage, A. *Angew. Chem., Int. Ed.* **2012**, *51*, 123−127.
(50) Vitzthum, V.; Miéville, P.; Carnevale, D.; Caporini, M. A.; Gajan, D.; Copéret, C.; Lelli, M.; Zagdoun, A.; Rossini, A. J.; Lesage, A.; Emsley, L.; Bodenhausen, G. *Chem. Commun.* **2012**, *48*, 1988−1990.
(51) Kobayashi, T.; Lafon, O.; Lilly Thankamony, A. S.; Slowing, I. I.; Kandel, K.; Carnevale, D.; Vitzthum, V.; Vezin, H.; Amoureux, J.-P.; Bodenhausen, G.; Pruski, M. *Phys. Chem. Chem. Phys.* **2013**, *15*, 5553−5562.
(52) Blanc, F.; Sperrin, L.; Jefferson, D. A.; Pawsey, S.; Rosay, M.; Grey, C. P. *J. Am. Chem. Soc.* **2013**, *135*, 2975−2978.
(53) Blanc, F.; Chong, S. Y.; McDonald, T. O.; Adams, D. J.; Pawsey, S.; Caporini, M. A.; Cooper, A. I. *J. Am. Chem. Soc.* **2013**, *135*, 15290−15293.
(54) Ouari, O.; Phan, T.; Ziarelli, F.; Casano, G.; Aussenac, F.; Thureau, P.; Gigmes, D.; Tordo, P.; Viel, S. *ACS Macro Lett.* **2013**, *2*, 715−719.
(55) Protesescu, L.; Rossini, A. J.; Kriegner, D.; Valla, M.; de Kergommeaux, A.; Walter, M.; Kravchyk, K. V.; Nachtegaal, M.; Stangl, J.; Malaman, B.; Reiss, P.; Lesage, A.; Emsley, L.; Copéret, C.; Kovalenko, M. V. *ACS Nano* **2014**, *8*, 2639−2648.
(56) Conley, M. P.; Rossini, A. J.; Comas-Vives, A.; Valla, M.; Casano, G.; Ouari, O.; Tordo, P.; Lesage, A.; Emsley, L.; Copéret, C. *Phys. Chem. Chem. Phys.* **2014**, *16*, 17822−17827.
(57) Gunther, W. R.; Michaelis, V. K.; Caporini, M. A.; Griffin, R. G.; Román-Leshkov, Y. *J. Am. Chem. Soc.* **2014**, *136*, 6219−6222.
(58) Lee, D.; Monin, G.; Duong, N. T.; Lopez, I. Z.; Bardet, M.; Mareau, V.; Gonon, L.; De Paëpe, G. *J. Am. Chem. Soc.* **2014**, *136*, 13781−13788.
(59) Zhang, J.; Scherer, G. W. *Cem. Concr. Res.* **2011**, *41*, 1024−1036.
(60) Golovastikov, N. I.; Matveeva, R. G.; Belov, N. V. *Sov. Phys.—Crystallogr.* **1976**, *20*, 441−445.
(61) Grangeon, S.; Claret, F.; Linard, Y.; Chiaberge, C. *Acta Crystallogr., Sect. B* **2013**, *69*, 465−473.
(62) Massiot, D.; Fayon, F.; Capron, M.; King, I.; Le Calvé, S.; Alonso, B.; Durand, J.-O.; Bujoli, B.; Gan, Z.; Hoatson, G. *Magn. Reson. Chem.* **2002**, *40*, 70−76.
(63) Hayashi, S.; Hayamizu, K. *Bull. Chem. Soc. Jpn.* **1991**, *64*, 685−687.
(64) Bemi, L.; Clark, H. C.; Davies, J. A.; Fyfe, C. A.; Wasylishen, R. E. *J. Am. Chem. Soc.* **1982**, *104*, 438−445.
(65) Pines, A.; Gibby, M. G.; Waugh, J. S. *J. Chem. Phys.* **1972**, *56*, 1776−1777.
(66) Zagdoun, A.; Casano, G.; Ouari, O.; Lapadula, G.; Rossini, A. J.; Lelli, M.; Baffert, M.; Gajan, D.; Veyre, L.; Maas, W. E.; Rosay, M.; Weber, R. T.; Thieuleux, C.; Copéret, C.; Lesage, A.; Tordo, P.; Emsley, L. *J. Am. Chem. Soc.* **2012**, *134*, 2284−2291.
(67) Zagdoun, A.; Casano, G.; Ouari, O.; Schwarzwälder, M.; Rossini, A. J.; Aussenac, F.; Yulikov, M.; Jeschke, G.; Copéret, C.; Lesage, A.; Tordo, P.; Emsley, L. *J. Am. Chem. Soc.* **2013**, *135*, 12790−12797.
(68) Song, C.; Hu, K.-N.; Joo, C.-G.; Swager, T. M.; Griffin, R. G. *J. Am. Chem. Soc.* **2006**, *128*, 11385−11390.
(69) Matsuki, Y.; Maly, T.; Ouari, O.; Karoui, H.; Le Moigne, F.; Rizzato, E.; Lyubenova, S.; Herzfeld, J.; Prisner, T.; Tordo, P.; Griffin, R. G. *Angew. Chem., Int. Ed.* **2009**, *48*, 4996−5000.
(70) Haze, O.; Corzilius, B.; Smith, A. A.; Griffin, R. G.; Swager, T. M. *J. Am. Chem. Soc.* **2012**, *134*, 14287−14290.
(71) Zagdoun, A.; Rossini, A. J.; Gajan, D.; Bourdolle, A.; Ouari, O.; Rosay, M.; Maas, W. E.; Tordo, P.; Lelli, M.; Emsley, L.; Lesage, A.; Copéret, C. *Chem. Commun.* **2012**, *48*, 654−656.
(72) During the course of this study, the TEKPol biradical was developed as a superior candidate for DNP NMR measurements that enables improved signal enhancements compared to those of bCTbK and was thereafter used for subsequent DNP NMR experiments.
(73) Rosay, M.; Tometich, L.; Pawsey, S.; Bader, R.; Schauwecker, R.; Blank, M.; Borchard, P. M.; Cauffman, S. R.; Felch, K. L.; Weber, R. T.; Temkin, R. J.; Griffin, R. G.; Maas, W. E. *Phys. Chem. Chem. Phys.* **2010**, *12*, 5850−5860.
(74) Fung, B. M.; Khitrin, A. K.; Ermolaev, K. *J. Magn. Reson.* **2000**, *142*, 97−101.
(75) Elena, B.; de Paëpe, G.; Emsley, L. *Chem. Phys. Lett.* **2004**, *398*, 532−538.
(76) Gullion, T.; Schaefer, J. *J. Magn. Reson.* **1989**, *81*, 196−200.
(77) Richardson, I. G. *Cem. Concr. Res.* **2008**, *38*, 137−158.
(78) Engelhardt, G.; Michel, D. *High-Resolution Solid-State NMR of Silicates and Zeolites*; John Wiley & Sons: Chichester, U.K., 1987.
(79) Jeffery, J. W. *Acta Crystallogr.* **1952**, *5*, 26−35.
(80) Skinner, L. B.; Chae, S. R.; Benmore, C. J.; Wenk, H. R.; Monteiro, P. J. M. *Phys. Rev. Lett.* **2010**, *104*, 195502.
(81) Allen, A. J.; Thomas, J. J.; Jennings, H. M. *Nat. Mater.* **2007**, *6*, 311−316.
(82) Pellenq, R. J.-M.; Kushima, A.; Shahsavari, R.; Van Vliet, K. J.; Buehler, M. J.; Yip, S.; Ulm, F.-J. *Proc. Natl. Acad. Sci. U.S.A.* **2009**, *106*, 16102−16107.
(83) Juenger, M. C. G.; Jennings, H. M. *Cem. Concr. Res.* **2002**, *32*, 393−399.
(84) Michel, F. M.; MacDonald, J.; Feng, J.; Phillips, B. L.; Ehm, L.; Tarabrella, C.; Parise, J. B.; Reeder, R. J. *Chem. Mater.* **2008**, *20*, 4720−4728.
(85) Akbey, Ü.; Franks, W. T.; Linden, A.; Lange, S.; Griffin, R. G.; van Rossum, B.-J.; Oschkinat, H. *Angew. Chem., Int. Ed.* **2010**, *49*, 7803−7806.
(86) Rosay, M.; Weis, V.; Kreischer, K. E.; Temkin, R. J.; Griffin, R. G. *J. Am. Chem. Soc.* **2002**, *124*, 3214−3215.
(87) The 1D $^{13}C\{^{1}H\}$ DNP CPMAS spectrum (Figure 5a, red) exhibits a ^{13}C signal centered at 40 ppm arising from alkyl ($-CH_2-$) moieties, which are likely associated with solvent impurities present in low concentrations.
(88) The biradical species could be present near the adsorbed sucrose molecules at silicate surfaces, consistent with the ^{13}C DNP signal enhancement profiles observed for the sucrose (Figure 5b) and solvent species (Supporting Information, Figure S2). Nevertheless, this results in negligible perturbation of the vast majority of surface-adsorbed sucrose species (within the sensitive detection limits of the DNP-NMR measurements), as indicated by comparison of the 1D $^{13}C\{^{1}H\}$ CPMAS spectra of tricalcium silicate with 0.1% bwos ^{13}C-sucrose without and with biradical solution (Supporting Information, Figure S3).
(89) Ayuela, A.; Dolado, J. S.; Campillo, I.; de Miguel, Y. R.; Erkizia, E.; Sánchez-Portal, D.; Rubio, A.; Porro, A.; Echenique, P. M. *J. Chem. Phys.* **2007**, *127*, 164710.
(90) Bellmann, F.; Damidot, D.; Möser, B.; Skibsted, J. *Cem. Concr. Res.* **2010**, *40*, 875−884.
(91) Bullard, J. W.; Jennings, H. M.; Livingston, R. A.; Nonat, A.; Scherer, G. W.; Schweitzer, J. S.; Scrivener, K. L.; Thomas, J. J. *Cem. Concr. Res.* **2011**, *41*, 1208−1223.
(92) Rejmak, P.; Dolado, J. S.; Stott, M. J.; Ayuela, A. *J. Phys. Chem. C* **2012**, *116*, 9755−9761.
(93) Youssef, M.; Pellenq, R. J.-M.; Yildiz, B. *J. Am. Chem. Soc.* **2011**, *133*, 2499−2510.
(94) Hunger, M. *Solid State Nucl. Magn. Reson.* **1996**, *6*, 1−29.
(95) Vega, A. J. *J. Am. Chem. Soc.* **1988**, *110*, 1049−1054.
(96) Janicke, M. T.; Landry, C. C.; Christiansen, S. C.; Kumar, D.; Stucky, G. D.; Chmelka, B. F. *J. Am. Chem. Soc.* **1998**, *120*, 6940−6951.
(97) Brunet, F.; Bertani, P.; Charpentier, T.; Nonat, A.; Virlet, J. *J. Phys. Chem. B* **2004**, *108*, 15494−15502.
(98) Pannetier, N.; Khoukh, A.; François, J. *Macromol. Symp.* **2001**, *166*, 203−208.
(99) Yesinowski, J. P.; Eckert, H.; Rossman, G. R. *J. Am. Chem. Soc.* **1988**, *110*, 1367−1375.
(100) Rassem, R.; Zanni-Théveneau, H.; Heidemann, D.; Grimmer, A. R. *Cem. Concr. Res.* **1993**, *23*, 169−176.

DOI: 10.1021/jacs.5b00622
J. Am. Chem. Soc. 2015, 137, 8096−8112

(101) Small quantities of 1,2-dichlorobenzene (frozen DNP solvent) are expected to also be present at or near the silicate particle surfaces (though associated $^{29}Si-^{1}H$ dipolar interactions are too weak to be detected in the 2D $^{29}Si\{^{1}H\}$ DNP HETCOR spectrum of Figure 6c). Because of the low (1.1%) natural isotopic abundance of ^{13}C moieties in 1,2-dichlorobenzene, they are unlikely to attenuate the ^{29}Si signals of silicate surface species in the DNP REDOR measurements. Within a hemispherical volume of radius ca. 10 Å from a ^{29}Si nucleus at the particle surface, the relative populations of ^{13}C nuclei associated with ^{13}C-labeled sucrose and the DNP solvent are estimated to be at least 100:1.

(102) Peterson, V. K.; Juenger, M. C. G. *Chem. Mater.* **2006**, *18*, 5798−5804.

(103) Mueller, K. T. *J. Magn. Reson., Ser. A* **1995**, *113*, 81−93.

(104) Sawada, K.; Araki, T.; Suzuki, T. *Inorg. Chem.* **1987**, *26*, 1199−1204.

(105) The sixth ionizable proton on NTMP is associated with the nitrilo nitrogen, which accounts for the large difference between the values of the fifth and sixth deprotonation constants (pK_a).

(106) Demadis, K. D.; Katarachia, S. D. *Phosphorus, Sulfur Silicon Relat. Elem.* **2004**, *179*, 627−648.

(107) Popov, K.; Rönkkömaki, H.; Lajunen, L. H. J. *Pure Appl. Chem.* **2001**, *73*, 1641−1677.

(108) An aqueous 5 wt% NTMP solution has a pH ∼1.

DOI: 10.1021/jacs.5b00622
J. Am. Chem. Soc. 2015, 137, 8096−8112